Liquid Crystals
Publication details, including instructions for authors and subscription information:
http://www.informaworld.com/smpp/title~content=t713926090

Determinate and stochastic orientation dynamics of nematic liquid crystals in the cross electric fields with frequencies up to the megahertz range

S. I. Trashkeev[a]; V. M. Klementev[a]; P. A. Statsenko[a]
[a] Institute of Laser Physics, Russian Academy of Sciences, Siberian Division, Novosibirsk 630090, Russia

To cite this Article Trashkeev, S. I. , Klementev, V. M. and Statsenko, P. A.(2006) 'Determinate and stochastic orientation dynamics of nematic liquid crystals in the cross electric fields with frequencies up to the megahertz range', Liquid Crystals, 33: 4, 417 — 438
To link to this Article: DOI: 10.1080/02678290600594539
URL: http://dx.doi.org/10.1080/02678290600594539

Liquid Crystals, Vol. 33, No. 4, April 2006, 417–438

Determinate and stochastic orientation dynamics of nematic liquid crystals in the cross electric fields with frequencies up to the megahertz range

S.I. TRASHKEEV*, V.M. KLEMENTEV and P.A. STATSENKO
Institute of Laser Physics, Russian Academy of Sciences, Siberian Division, Novosibirsk 630090, Russia

(*Received 22 April 2005; in final form 1 December 2005; accepted 1 December 2005*)

A theoretical and experimental description is given of the director orientation dynamics in nematic liquid crystals placed in variable electric fields comprising several components and having different directions (crossed fields) and frequencies up to 5 MHz. The calculations show that the system of interest is a physical object governed by non-linear dynamics. Depending on numerical values of governing parameters, the following director state regimes are obtained: stationary, periodic, quasi-periodic (multi-modal), and stochastic strange-attractor-type. In the calculations, all the states are obtained by solving a determinate system of two time-dependent first order non-linear equations, ignoring the electrohydrodynamic effect. Preliminary verification is performed, and qualitative agreement with the mathematical model under consideration is obtained in the range of frequencies (approximately 100 Hz and higher) that allows electrical conductivity to be ignored. The influence of 2D and 3D rotating electric fields with one frequency, and two- or three-component fields with different frequencies, in the interval from 10 Hz to 5 MHz on the orientation of a nematic liquid crystal is considered.

1. Introduction

Electro-optical properties of liquid crystals (LCs) are at present well understood and have been studied in detail in numerous publications and monographs, [1–4]. From the practical point of view, LCs have found wide application in data display [2], which is based on the reorientation of the LC director and optical axis of the medium, under the action of electric fields of low strength—the Fréedericksz effect [1]. As a rule, the time characteristics of Fréedericksz reorientations are long, amounting to ~10–100 ms for a nematic LC (NLC) [3]. This response speed of the electro-optical changes in a NLC results from the high rotational viscosity (0.1–1 P) [3], which is inherent in almost any liquid crystal. That is why it is supposed that at frequencies of $\geqslant$100 Hz, the director re-orientation depends mainly on the viscosity and root-mean-square value of the variable electric field, and only weakly on its frequency. Hence it is concluded that high-frequency reorientation in a LC is impossible [5].

The purpose of the present study was to examine qualitatively the orientational behaviour of a NLC in electric fields comprising several components with different directions (crossed field) and frequencies. In such fields the director motion depends on the amplitudes, frequencies and phases of the imposed voltages, presenting continuous multi-frequency (quasi-periodical) oscillating or rotating changes of orientation, up to those close to the stochastic regimes of the strange attractor type. By its nature, the dynamics of the processes under study does not result from mere electrohydrodynamic (EHD) instability [4], since we have considered frequencies up to 5 MHz. Typical macroscopic flows of the liquid were observed at frequencies of about 10 Hz, or at the instant of external voltage cut-in and cut-off. Theoretical conclusions have been proven qualitatively by previous experimental data.

The first mention of the possible stochastization of the NLC orientation state with no EHD-effect is found in [6], where the authors studied experimentally the interaction between the NLC and ordinary type light waves of oblique incidence. Later, they studied the determination of equations for the basic numerical calculations [7] and revealed the possibility of quasi-periodical and multi-mode regimes in the models, describing the experiment in [6]. The study of this phenomenon was continued in [8].

The early studies with the NLC in rotating magnetic and electric fields were carried out by Tzvetkov and co-workers [9]; the purpose was to define viscous constants. The papers of B. Meyer *et al.* [10, 11] are very close to the topic. They are devoted to the behaviour of NLC

*Corresponding author. Email: sitrskv@mail.ru

Liquid Crystals
ISSN 0267-8292 print/ISSN 1366-5855 online © 2006 Taylor & Francis
http://www.tandf.co.uk/journals
DOI: 10.1080/02678290600594539

orientation in 2D rotating magnetic fields with low frequencies, under or about several dozens hertz. In that work the authors point out that it is necessary to observe the hydrodynamic streams, which appear at the low frequency reorientation from the homeotropic initial state of the NLC. Among recent papers, we should mention [12], which considers the similar mechanism of the high speed director reorientation (frequency of about 10 kHz, peak voltage about 200 V) in 2D rotating electric fields. Some issues of rotating and stochastic NLC orientation in multi-component high frequency electric fields (including 3D rotating fields), are described in [13], where questions of pumping laser systems in the tera-Hertz range with a liquid crystal active medium, in the dielectric regime, were studied.

The early experiments of the present paper do not aim to describe fully the whole body of possible orientation phenomena that appear in a NLC interacting with variable electric fields of complex configuration. The purpose is to prove qualitatively conclusions derived from the approximate mathematical model. This is the problems statement, and investigations will be continued in the future.

2. Equations of motion

To derive dynamic equations, we consider the interaction geometry presented in figure 1; in the Cartesian coordinate system $\mathbf{r}=(x, y, z)$. The designations are: $\mathbf{E}=\mathbf{E}(t, \mathbf{r})$ is the real-valued electric field vector in the crystal, $\mathbf{n}=\mathbf{n}(t, \mathbf{r})$ is the unit vector (director), and θ and φ are, respectively, the polar and azimuth angles, related to $\mathbf{n}$ by the formula:

$$\mathbf{n}=(n_x, n_y, n_z)=(\sin\theta\cos\varphi, \sin\theta\sin\varphi, \cos\theta). \quad (1)$$

Next, we conveniently introduce the following unit vectors orthogonal to $\mathbf{n}$:

$$\mathbf{m}=(m_x, m_y, m_z)=\frac{\partial\mathbf{n}}{\partial\theta}=(\cos\theta\cos\varphi, \cos\theta\sin\varphi, -\sin\theta)$$
$$\mathbf{p}=(p_x, p_y, p_z)=\frac{1}{\sin\theta}\frac{\partial\mathbf{n}}{\partial\varphi}=(-\sin\varphi, \cos\varphi, 0) \quad (2)$$
$$(\mathbf{nm})=0, (\mathbf{np})=0, (\mathbf{mp})=0.$$

The volumetric part of the free energy density F for the NLC is written as in [1]:

$$F=\frac{1}{2}\left[K_1(\operatorname{div}\mathbf{n})^2+K_2(\mathbf{n}\operatorname{rot}\mathbf{n})^2+K_3(\mathbf{n}\times\operatorname{rot}\mathbf{n})^2\right] - \frac{\varepsilon_a}{8\pi}(\mathbf{nE})^2. \quad (3)$$

Here, K_1, K_2, K_3 are the Frank elastic constants; and $\varepsilon_a=\varepsilon_\parallel-\varepsilon_\perp$, and $\varepsilon_\parallel$, $\varepsilon_\perp$ are the parameters of the dielectric transmissivity tensor, which can be expressed in terms of the Cartesian components n_i of the director as follows:

$$\varepsilon_{ij}=\varepsilon_\perp\delta_{ij}+\varepsilon_a n_i n_j, \quad i, j=x, y, z, \quad (4)$$

where δ_{ij} is the Kronecker delta. The surface terms of the free energy dictate the type of boundary interaction, and their contribution is limited by the boundary conditions.

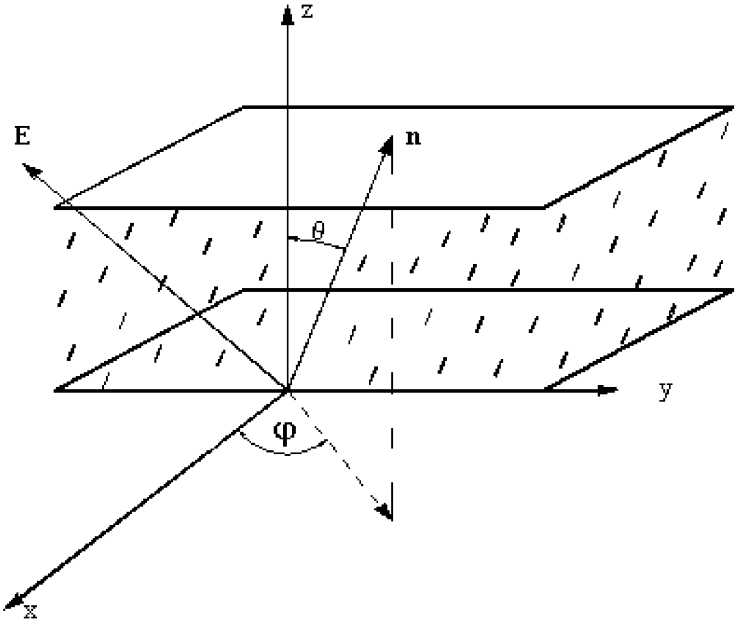

Figure 1. Geometry of the NLC director interaction with an arbitrarily directed electric field.

In the following we will consider the frequencies of the electric fields, which influence the NLC and do not differ very much from each other. We ignore the frequency dependence of the material parameters K_i, $\varepsilon_{\|}$, $\varepsilon_{\perp}$. For MBBA, except for the region of anisotropy sign inversion (about 15 MHz), a frequency deviating by 10% causes a change in dielectric constants of less than 0.1–1% [4]. For 5CB in the frequency range under consideration, the deviation is even less. There are no data for the dispersion of the elastic and viscous parameters.

In the 1D case, when all sought values depend only on the coordinate z, expression (3) is written as follows:

$$F = \frac{1}{2}\left[f\left(\frac{\partial\theta}{\partial z}\right)^2 + g\left(\frac{\partial\varphi}{\partial z}\right)^2 - \frac{\varepsilon_a}{4\pi}(\mathbf{nE})^2\right] \tag{5}$$

where

$$f = f(\theta) = K_1 \sin^2\theta + K_3\cos^2\theta,$$
$$g = g(\theta) = \sin^2\theta\left(K_2\sin^2\theta + K_3\cos^2\theta\right).$$

Variation in equation (5), taking into account the relaxation terms, which dictate the time dependence t, yields the following system of two nonlinear equations for θ and φ [4]:

$$\gamma\frac{\partial\theta}{\partial t} = f\frac{\partial^2\theta}{\partial z^2} + \frac{1}{2}\left[f_\theta\left(\frac{\partial\theta}{\partial z}\right)^2 + g_\theta\left(\frac{\partial\varphi}{\partial z}\right)^2\right] + \frac{\varepsilon_a}{4\pi}(\mathbf{nE})\,(\mathbf{mE})$$
$$\gamma\sin^2\theta\frac{\partial\varphi}{\partial t} = \frac{\partial}{\partial z}\left(g\frac{\partial\varphi}{\partial z}\right) + \frac{\varepsilon_a}{4\pi}\sin\theta(\mathbf{nE})(\mathbf{pE}). \tag{6}$$

Here, $f_\theta = \partial f/\partial\theta$, $g_\theta = \partial g/\partial\theta$, and γ is the viscosity parameter of the NLC. The special case resulting from the system of equations (6) is considered in [10], when the electric fields are changed to magnetic fields. Equations (6) are written in the approximation, that does not take account of the flexoelectric additives or the EHD-transfer of the liquid, which can be ignored when a quite pure NLC is influenced by high frequency electric fields. Conductivity in liquids is caused by the fluidity of the ionic impurities and as a rule decreases rapidly as the electric field frequency rises. The counter-flows, especially during reorientation from the initial homeotropic state [1, 4], will significantly affect the director state at high frequency only at the start and stop moments of the electric field, or for some other reasons (as indicated below), which promote the low frequencies in the dynamics of NLC orientation. In the context of the accepted approximations, the equations (6) are correct at frequencies above 100 Hz [3, 4]. We have also considered experimentally the lower frequencies of some dozens Hertz. In this region the EHD application is incorrect. The flexoelectricity and hydrodynamics, with more accurate definition of the applicability boundaries, calls for individual study.

To the material equations (6) are to be added the appropriate boundary conditions at $z=0$, L, where L is the crystal thickness. We adopt the following conditions [4]:

$$\left[K\frac{\partial\theta}{\partial z} \pm a_\theta\theta\right]_{z=0,\,L} = b_\theta, \quad \left[K\frac{\partial\varphi}{\partial z} \pm a_\varphi\varphi\right]_{z=0,\,L} = b_\varphi \tag{7}$$

where the signs $\pm$, respectively, refer to the planes $z=0$ and $z=L$; K is the mean Frank constant, and the parameters a_θ, a_φ, b_θ, b_φ generally depend on the surface energy density of the director with the bounding planes, the flexo-electric coefficients and the electric-field intensity.

To obtain a closed system, Maxwell equations establishing the relationship between the electric fields and the orientation of **n** should be added to (6). In the context of the accepted approximations in the sample, the necessary relationship is written in the dielectric mode:

$$\mathrm{div}\left(\hat{\varepsilon}\mathbf{E}\right) = 0, \quad \mathrm{rot}\,\mathbf{E} = 0. \tag{8}$$

Here $\hat{\varepsilon}$ is the transmissivity tensor defined by (4). In the one-dimensional case, with (4), equations (8) acquire the form

$$\frac{\partial}{\partial z}\left[\varepsilon_\perp E_z + \varepsilon_a n_z(\mathbf{nE})\right] = 0, \quad \frac{\partial E_x}{\partial z} = \frac{\partial E_y}{\partial z} = 0. \tag{9}$$

Equations (9) are easily integrated and the electric fields inside the crystal can be uniquely determined from specified field values. With appropriate initial conditions for orientation angles,

$$\theta(0, z) = \theta_0(z), \quad \varphi(0, z) = \varphi_0(z) \tag{10}$$

we obtain the closed system (6) with boundary conditions (7) and the solution may be obtained with allowance for (9); this system can be used to predict the NLC interaction with the variable electric field in a one-dimensional case.

Considering sufficiently intense electric fields, which do not depend on the spatial coordinates and excess threshold values for the Fréedericksz reorientation [1], we have

$$|\mathbf{E}|^2 >> E_{th}^2 = \frac{4\pi^3 K_3}{L^2\varepsilon_a}. \tag{11}$$

Then the coordinate dependences can be ignored inside the region, except for the thin near-surface layers, and the boundary conditions effect is neglected [1, 9, 10].

The simplified equations (6) and (9) yield a system of ordinary differential equations depending on time only:

$$\gamma\frac{d\theta}{dt}=\frac{\varepsilon_a}{4\pi}(\mathbf{nE})(\mathbf{mE}),\quad \gamma\sin\theta\frac{d\varphi}{dt}=\frac{\varepsilon_a}{4\pi}(\mathbf{nE})(\mathbf{pE}),$$
$$E_z=\frac{\varepsilon_\parallel E_z^{ex}-\varepsilon_a\cos\theta\sin\theta\left(E_x\cos\varphi+E_y\sin\varphi\right)}{\varepsilon_\perp+\varepsilon_a\cos^2\theta},\qquad(12)$$
$$E_x=E_x^{ex},\quad E_y=E_y^{ex},$$
$$\theta(0)=\theta_0,\quad \varphi(0)=\varphi_0$$

where $\theta=\theta(t)$, $\varphi=\varphi(t)$ are the angle functions in the central part of the sample ($z\cong L/2$), θ_0, φ_0 are their primary values, $\mathbf{E}^{ex}(t)$ are the external electric fields in the absence of a medium. The assumption of coordinate independence of the external electric fields with changing spatial direction is incorrect in the general case. It is valid if we consider the sample region, whose typical size is much smaller than the size of the fields' non-uniformity.

3. 2D Electric field: analytical solution

The system of equations (6) and simplified system (12) in some cases allowing to carry out analytical research, but the general case demands numerical calculation. First we consider the case with the analytical solution. Let us consider the vector of the electric field $\mathbf{E}=\mathbf{E}(t)$, which lies in the plane (x, y). Here, at $\theta\equiv\pi/2$, $\varphi=\varphi(t)$, $\mathbf{E}=[E_x(t), E_y(t), 0]$, instead of the system (12) equations we have one equation for the horizontal angle φ of ($E_z\equiv0$) kind:

$$\gamma\frac{d\varphi}{dt}=\frac{\varepsilon_a}{4\pi}\left(E_x\cos\varphi+E_y\sin\varphi\right)\left(-E_x\sin\varphi+E_y\cos\varphi\right)\quad(13)$$

In the case of periodic time dependence $\mathbf{E}(t)=A[\sin(\omega t+\psi_x), \sin(\omega t+\psi_y), 0]$, for the 2D rotating (circular) field $E_x=A\cos\omega t$, $E_y=\sin\omega t$ ($\psi_x=\pi/2$, $\psi_y=0$) we have [10]

$$\frac{d\varphi}{dt}=-\frac{\varepsilon_a A^2}{8\pi\gamma}\sin[2(\varphi-\omega t)].\qquad(14)$$

If we consider the field $\mathbf{E}(t)=A[\cos(\omega t), 0, \sin(\omega t)]$, which lies in the plane (x, z), then, from (12), at $\varphi\equiv0$, for the polar angle $\theta=\theta(t)$, we obtain an equation similar to (14).

Equation (14) is integrated analytically. Let us define $\alpha=2(\varphi-\omega t)$ and turn to the dimensionless time $\tau=\omega t$; then (14) will be written as

$$\frac{d\alpha}{d\tau}=-2(1+\delta\sin\alpha).\qquad(15)$$

Thus we obtain the solution

$$\varphi(\tau)=\begin{cases}\tau-arctg[\delta+\Omega tg\Omega(\tau-C)], & \delta^2<1, \quad \Omega^2=1-\delta^2,\\ \tau-arctg\left(\frac{\tau-1-C}{\tau-C}\right), & \delta^2=1, \quad \Omega^2=0,\\ \tau-arctg[\delta-\Omega th\Omega(\tau-C)], & \delta^2>1, \quad \Omega^2=\delta^2-1,\end{cases}\qquad(16)$$

where $\delta=\varepsilon_a A^2/(8\pi\gamma\omega)$, and constant C is defined from the initial conditions. The action of the time-linear term in equations (16), which results in a continuous, on average, rotation of the director, is cancelled.

For comparison, we present here the solution of equation (13) for the case of a unidirectional electric field $\mathbf{E}$: $E_x=A\sin\omega t$, $E_y=A\sin\omega t$, $E_z=0$ ($\psi_x=\psi_y=0$). It follows from equation (13) that

$$\frac{d\varphi}{dt}=\frac{\varepsilon_a A^2}{4\pi\gamma}\sin^2\omega t\cos2\varphi.\qquad(17)$$

Equation (17) can also be easily integrated; the solution is

$$\varphi=-\frac{\pi}{4}\pm arctg\{C\exp[\delta(2\tau-\sin2\tau)]\}\qquad(18)$$

where C is the integration constant, and the dimensionless time τ and the parameter δ are defined as previously. Relationship (18) describes non-threshold Fréedericksz reorientation in a variable electric field.

Let us consider the behaviour of φ for both cases of the field configuration in the onset mode ($\tau\to\infty$) and under the condition $\delta^2\ll1$ or $\omega\gg\varepsilon_a A^2/8\pi\gamma$. For the rotating field, we have from equation (16)

$$\varphi_1\approx C_1+\frac{\varepsilon_a A^2}{8\pi\gamma\omega}\sin2\omega t+\frac{1}{\omega}\left(\frac{\varepsilon_a A^2}{8\pi\gamma}\right)^2 t\qquad(19)$$

where, as can be seen, there are oscillating and time-linear items. For the second case, it follows from (18) that

$$\varphi_2\approx C_2+\frac{\varepsilon_a A^2}{4\pi\gamma\omega}\exp\left(-\frac{\varepsilon_a A^2}{4\pi\gamma}t\right)\sin^2\omega t.\qquad(20)$$

As can be seen from equation (19) and (20), in the case of a circular field the amplitude of director oscillations in the solution of φ_1 is finite in time; in a unidirectional field, for φ_2, this amplitude vanishes as $t\to\infty$. The integration constants C_1, C_2 do not depend on time. This undamped oscillatory behaviour of the director orientation, and also the continuous rotation of the director with a frequency proportional to the fourth power of the supplied voltage amplitude A, is a qualitative property of the case considered (19), which distinguishes it from the non-threshold Fréedericksz transition in variable fields with constant direction equation (20).

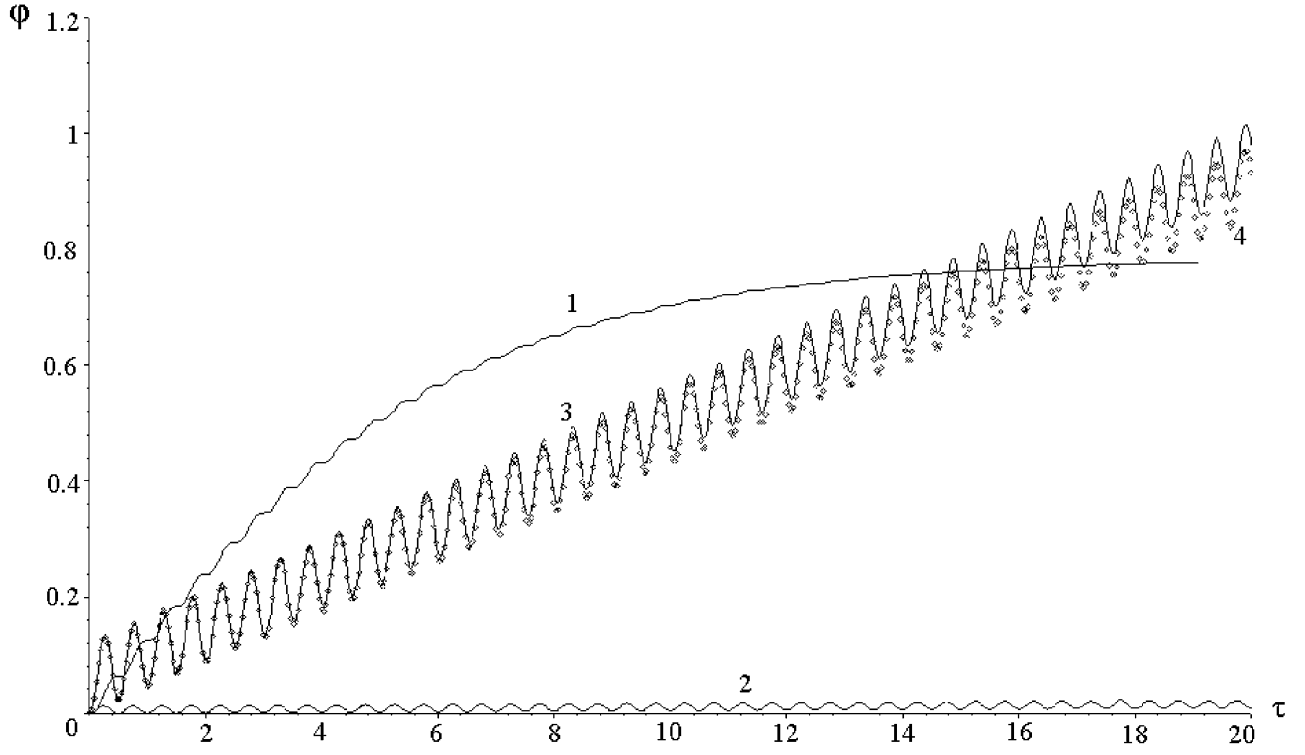

Figure 2. Dependence of the azimuth angle in radian of the NLC director orientation on the dimensionless time τ for the case of a 2D electric field lying in the plane (x, y). Curve 1: $\psi_x-\psi_y=0$, $\delta=0.5$; curve 2: $\psi_x-\psi_y=\pi/2$, $\delta=0.3$; curve 3: $\psi_x-\psi_y=\pi/2$, $\delta=3$; curve 4: (rhombs) $\psi_x-\psi_y=\pi/2$, $\delta=3$, the solution for medium elasticity.

The possibility of continuous director rotation was discovered and examined in [14]; these authors studied the interaction of homeotropically oriented nematics with circularly polarized light waves. Taking into account the mentioned approximations, the case (19) qualitatively approaches the results given in [14], in spite of the fact that light-induced reorientation has its own features.

Figure 2 presents the solutions $\varphi(\tau)$ for different δ, which follow from equation (17): curve 1 involves dependence (18) and equation (14); curves 2, 3 involve dependence (16). For comparison, the rhombs (curve 4) present the numerical solution in the sample centre $\varphi(\tau)\equiv\varphi(\tau, L/2)$, which follows from the equations in partial derivatives (6) for the case of the electric field rotating in the plane (x, y). The boundary conditions were chosen for homeotropic orientation and are written as

$$\theta|_{0,L}=0, \quad \frac{\partial\varphi}{\partial z}|_{0,L}=0.$$

Curve 3 is derived at $\delta=3$, curve 4 is for the value of the field amplitude, which is twice the threshold value, $|\mathbf{E}|=2E_{\text{th}}$ (such a field allows one to compare the calculation variants). In the context of the accepted approximations, both variants must give solutions close to each other. As is seen in from curves 3 and 4, taking account of the spatial dependences, which are dictated by the elastic forces in the NLC, results in a slight change of the inclination angle of the average values of φ to axis τ. Figure 3 demonstrates the calculated function of transmission $T(\tau)$ under crossed polarizers for the solution shown by curve 3 in figure 2. The smooth envelope $T(\tau)$ is caused by the continuous rotation of the director. It depends on the linear term in the solution to equation (16). The high frequency component depends on the oscillating additive to (16).

In the case when the field rotates in the plane (x, z), solutions for the versions with and without NLC elasticity start to differ more significantly than in the previous example. Figure 4 shows the dependences of the polar angle $\theta(\tau)$ obtained from the integrated system of ordinary differential equations (12), which trans form to equation (14), φ changes to θ (curve 1); and from the solved system of equations in partial derivatives (6) in the case when $\varphi=0$ (curve 2), with due regard to the medium elasticity for $\theta(\tau)\equiv\theta(\tau, L/2)$. The boundary conditions for (6) were similar to the previous case. Curve 1 corresponds to $\delta=3$. For curve 2 (rhombs), the value of the field amplitude exceeded the threshold

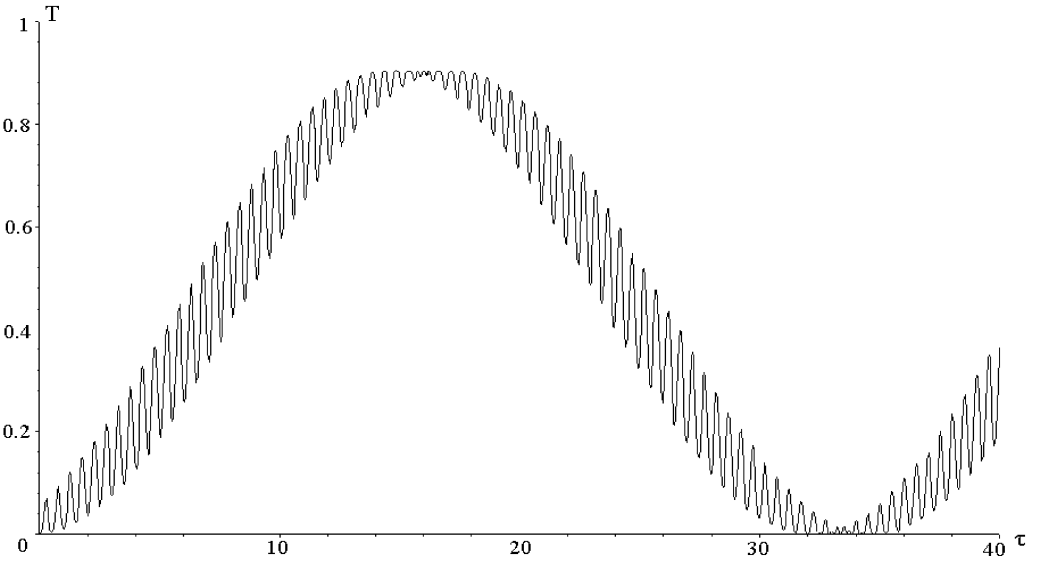

Figure 3. Dependence of the NLC transmission function on the dimensionless time in the rotating field mode at $\psi_x-\psi_y=\pi/2$, $\delta=3$ (for the solution shown by curve 3, figure 2).

value by 5.5 times. Curve 2 in figure 4 oscillates with the same frequency and amplitude as curve 1, and on average shows a stationary level dictated by the field amplitude A, elastic constants and thickness of the crystal L. Numerical analysis of equations (6) for the case of the field rotating in plane (x, z) revealed the impossibility of continuous rotation of the director, even at an arbitrarily large excess of the field amplitude value over the threshold value (it also follows from the qualitative concept). Hence, figure 4 illustrates the case

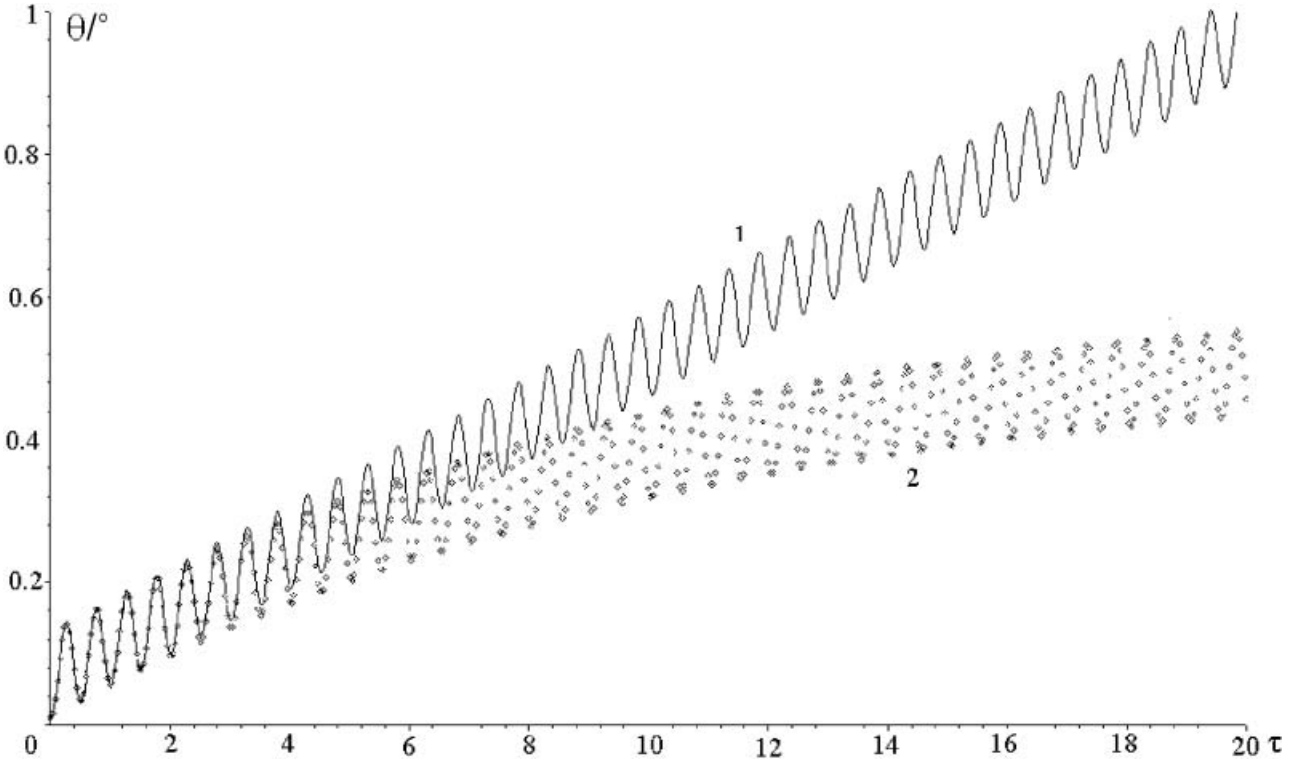

Figure 4. Dependence of the polar angle in radian of the NLC director orientation on the dimensionless time for the case of a 2D circular electric field ($\psi_x-\psi_z=\pi/2$, $\delta=3$) lying in the plane (x, z): curve 1, elasticity ignored; curve 2 (rhombs), elasticity included.

Table 1. Initial parameters for the numerical calculation.

	a	N	ψ	
Figure number	a_x:a_y:a_z	N_x:N_y:N_z	ψ_x, ψ_y, ψ_z	δ
5	1:1:0	1:1:1	0, $\pi/2$, 0	3
6	1:1:0	1:0.85:0	–	3
7, 9	1:1:1	1.25:1:1	0, $\pi/2$, 0	−1.5
8, 12	1:1:1	1:1.1:1	0, 0, $\pi/2$	0.65
10, 11	1:1:1.5	1:1.1:1	$\pi/2$, 0, 0	30
13(*a*), 13(*b*)	1:1.1:1	1.25:1.1:1	0, $\pi/2$, 0	−5
13(*c*), 13(*d*)	1:1:1.06	1.2:1:1	0, $\pi/2$, 0	−2
13(*e*), 13(*f*)	1:1:1	1:1.1:1	$\pi/2$, 0, 0	−1.45

when the ignored spatial dependences may distort qualitatively the pattern of the orientation dynamics. A detailed study of NLC director reorientation, taking account of spatial dependences and accuracy of the approximations, accepted in the present paper, will be reported in future papers.

4. NLC 3D orientational dynamics: numerical modelling

To solve the system of equations (12) in the general case, we used numerical solution. The electric field values were assigned as follows:

$$E_x = E_{x\mathrm{o}} \sin(2\pi v_x t + \psi_x), \quad E_y = E_{y\mathrm{o}} \sin\left(2\pi v_y t + \psi_y\right)$$
$$E_z = \frac{\varepsilon_{\|} E_{z\mathrm{o}} \sin(2\pi v_z t + \psi_z) - \varepsilon_{\mathrm{a}} \sin\theta\cos\theta\left(E_x\cos\varphi + E_y \sin\varphi\right)}{\varepsilon_{\perp} + \varepsilon_{\mathrm{a}}\cos^2\theta} \quad (21)$$

where E_{x0}, E_{y0}, E_{z0} are the amplitudes of the electric fields in vacuum. In the z-component of the electric field, the anisotropic additive resulting from condition (9) of the Maxwell equations was used; $\omega_i = 2\pi v_i$. For calculations, system (12) can be transformed to cyclic frequency and re-written as:

$$\frac{\mathrm{d}\theta}{\mathrm{d}\tau} = \delta(\mathbf{nA})(\mathbf{mA}), \quad \sin\theta\frac{\mathrm{d}\varphi}{\mathrm{d}\tau} = \delta(\mathbf{nA})(\mathbf{pA}),$$
$$\theta(0) = \theta_0, \quad \varphi(0) = \varphi_0 \quad (22)$$

where θ_0 and φ_0 are the initial conditions. As normalization factors, the root-mean-square field amplitude $A = \left(E_{x\mathrm{o}}^2 + E_{y\mathrm{o}}^2 + E_{z\mathrm{o}}^2\right)^{1/2}$ and the mean frequency $v_0 = (v_x + v_y + v_z)/3$ were used. Then

$$A_x = a_x \sin(2\pi N_x \tau + \psi_x), \quad A_y = a_y \sin\left(2\pi N_y \tau + \psi_y\right),$$
$$A_z = \frac{\varepsilon_{\|} a_z \sin(2\pi N_z \tau + \psi_z) - \varepsilon_{\mathrm{a}} \sin\theta\cos\theta\left(A_x\cos\varphi + A_y\sin\varphi\right)}{\varepsilon_{\perp} + \varepsilon_{\mathrm{a}}\cos^2\theta} \quad (23)$$

where $a_x = E_{x\mathrm{o}}/A$, $a_y = E_{y\mathrm{o}}/A$, $a_z = E_{z\mathrm{o}}/A$; $N_x = v_x/v_0$, $N_y = v_y/v_0$, $N_z = v_z/v_0$; and ψ_x, ψ_y, ψ_z are the phase additives. The dimensionless time is $\tau = v_0\, t$ and $\delta = \varepsilon_{\mathrm{a}} A^2/(4\pi\gamma v_0)$.

The solutions to equation (22) behave rather differently. Depending on the parameter values, the following regimes were observed: attainment of a stationary solution (analogue of the non-threshold Fréedericksz transition), periodic regime, quasi-periodic (multimodal) regime, and stochastic regimes of the strange-attractor type. By way of illustration, we present here several designs of dynamic orientation regime, which clearly reflect the complexity of the predicted dependences. Along with the functions $\theta(\tau)$ and $\varphi(\tau)$ found, the behaviour of the solution with time can be determined by considering the motion of the end of the vector **n** on a unit sphere or the trajectory of this motion on the plane (θ, φ), which represents an analogue of the phase space, the spectral characteristics of the design solutions, and the spectrum of the transmission function of the NLC sample. The latter characteristic is important, since it is registered experimentally in the simplest manner. The initial parameters, for which the design has been carried out and curves constructed, are listed in table 1.

The transmission function T is obtained from the intensity of the light passing though the NLC. In general, for the optical axis, which coincides with **n**, arbitrarily directed in space, T appears as [15]:

$$T(\tau) = T[\theta(\tau), \varphi(\tau)] = \cos^2\chi - \sin 2\varphi \sin 2(\varphi - \chi)\sin^2\frac{\Delta}{2}. \quad (24)$$

The difference of phase incursion Δ, which ignores the spatial dependences, is calculated from the formula

$$\Delta = 2\pi\frac{L}{\lambda}\left[\frac{n_{\perp} n_{\|}}{\left(n_{\perp}^2\cos^2\theta + n_{\|}^2\sin^2\theta\right)^{\frac{1}{2}}} - n_{\perp}\right]$$

where λ is the wavelength of the normally incident probe radiation, $n_{\|}$, $n_{\perp}$ are the major values of the

refractive indices for ordinary and extraordinary waves, respectively, and χ is the angle between the polarizer and analyser For the case of $\chi=\pi/4$, $\theta=0$, $T(\tau)$ becomes

$$T(\tau)=T[\varphi(\tau)]=[1+\sin 4\varphi(\tau)]/2. \qquad (25)$$

The Fourier-transformation F[$T(\tau)$] is used to analyse the spectral characteristics of $T(\tau)$. The frequency maxima that characterize the dynamics of orientation **n** must be present in the spectrum $T(\tau)$; it will change in accordance with equation (24), (25). The director rotation, time-linear part in the $\varphi(\tau)$ dependence (16) or (19), must contribute, in accordance with equation (25) to the Fourier-spectrum F[$T(\tau)$] in the area where the frequency is four times the rotation frequency **n**. The oscillating additives in equation (16) or (19) can change the spectral composition F[$T(\tau)$] as compared with the Fourier-spectra F[$\varphi(\tau)$], F[$\theta(\tau)$], but the major part of the oscillations must remain almost the same.

Figure 5 shows the designed absolute value |F[$T(\tau)$]| of the transmission function spectrum dimensionless frequency $N=\nu/\nu_0$ at $\delta=3$ for a single-frequency 2D rotating field, figure 6 shows the same characteristic for a two-component two-frequency field at the same $\delta=3$. In the first version, figure 5 (*a*), there is a pronounced peak at the frequency $N=2$, which correlates with the director oscillations (16) and on the shifted $N\sim1.97$. This shift results from the modulation of transmission function by the director rotation. The frequency component caused by the rotation of **n** is shown in figure 5 (*b*) for $0\leqslant N\leqslant 0.1$, it is equal to the fourfold director rotation frequency (figure 2, curve 3). In the second version (figure 6), under the action of the two-frequency field ($N_x=1$, $N_y=0.85$), we observe: the maximum at the doubled differential frequency $2(N_x-N_y)$, the harmonics divisible to this frequency, and the peaks on the doubled frequencies of the external fields. All design graphs of the transmission function are normalized to 1 at the maximum point. The maxima in figures 5 and 6 correlates with zero frequency.

Figures 7–13 (see also table 1) show the solutions of equation (22) for two types of NLC, which have ε_a of different sign, which dictates the sign of the dimensionless parameter δ. As can be seen from the Figures, the behaviour of the director orientation with time can present complex quasi-periodic and stochastic trajectories analogous to solutions of the strange-attractor type [16]. Depending on initial parameters, the director may have several limiting states (limiting cycles [16]), around which it performs an oscillatory or rotational motion, maving, periodically or quasi-periodically, from one cycle to another (figure 7). In the given example, the high frequency component, whose amplitude considerably increases at the moment of transition from one state to another, is implied in slow periodical changes of the orientation angle state. The mean values of neighbouring levels with respect to $\varphi(\tau)$ differ from each other by $\pm\pi$, the sign of the jump being random. The maximum values of $\theta(\tau)$, about $\pi/2$, are attained at

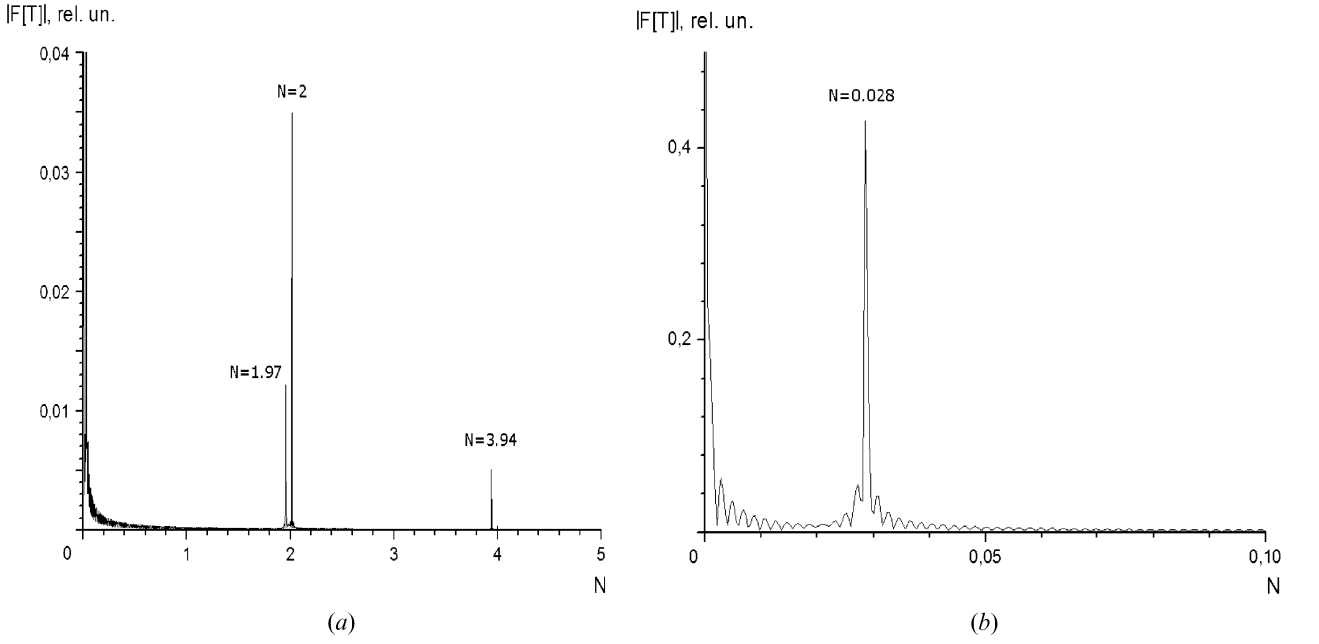

Figure 5. Designed module of the transmission function spectrum vs dimensionless frequency for a 2D field rotating in the plane (x, y); $\psi_x-\psi_y=\pi/2$, $\delta=3$. (*a*) frequency range $0\leqslant N\leqslant 5$; (*b*) $0\leqslant N\leqslant 0.1$, showing the peak responsible for the director rotation.

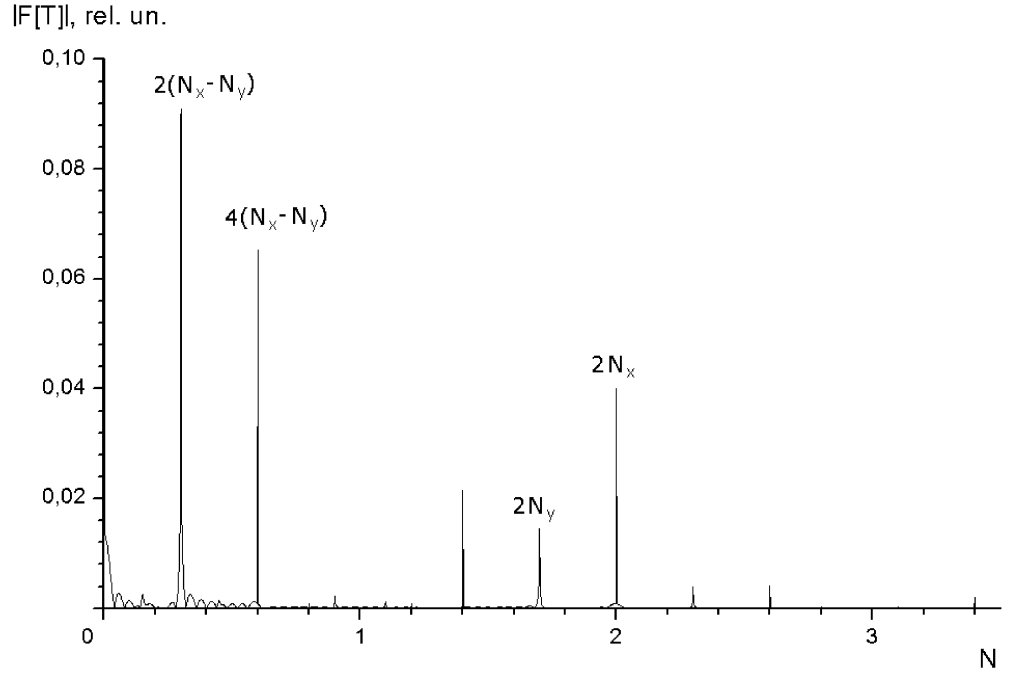

Figure 6. Designed module of the transmission function spectrum vs dimensionless frequency for a 2D two-frequency field in the plane (x, y); $N_x=1$, $N_y=0.85$, $\delta=3$.

the triangle vertices. Unlike the function $\varphi(\tau)$, the high frequency amplitude of $\theta(\tau)$ is observed less clearly on the background of the smoother variations.

In such regimes, the solutions of the equations depend on initial conditions. By way of example, figure 8 shows the curves $\varphi(\tau)$ predicted for various zero-time conditions $\theta(0)$ and $\varphi(0)$ (to improve the clarity of the figure, the dependences $\theta(\tau)$ are not shown). The figure shows that at a moment close to $\tau=0$, the curves $\varphi(\tau)$ behave similarly for various initial

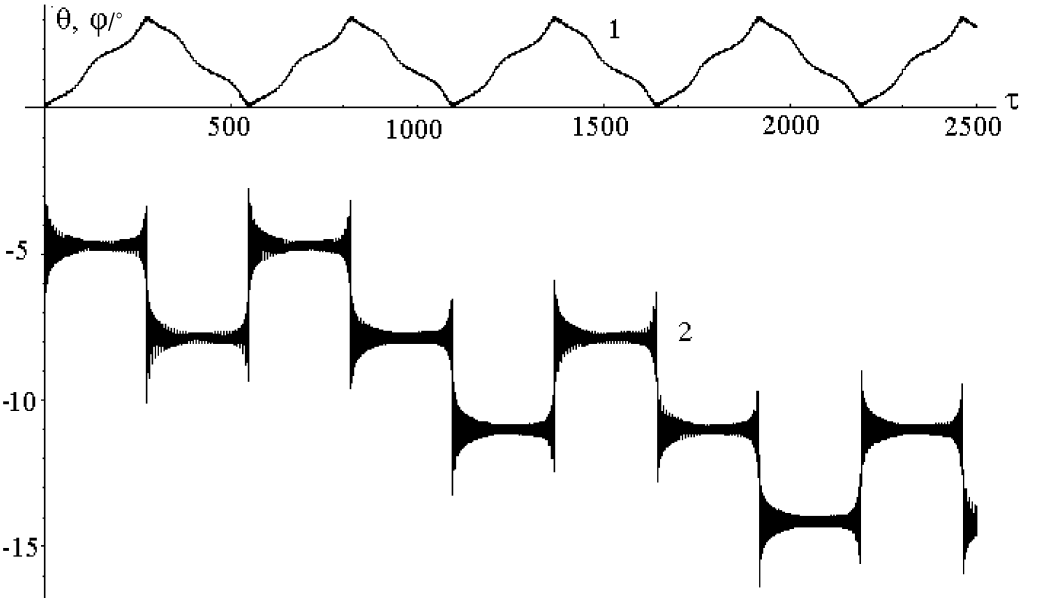

Figure 7. Dependence of the polar angle θ (curve 1) and azimuthal angle φ (curve 2) in radian of the director orientation on dimensionless time. Design parameters of the fields are listed in table 1.

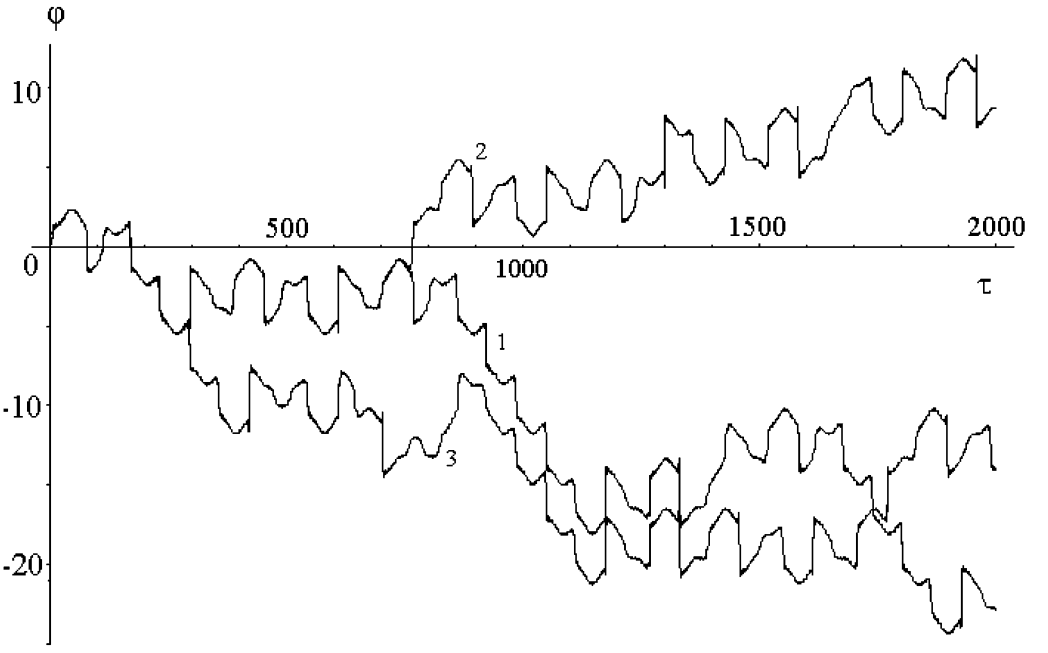

Figure 8. Dependence of the azimuth angle φ in radian on the dimensionless time τ under different initial conditions: curve 1 – $\theta_0 = 0.001$, $\varphi_0 = 0$; curve 2 – $\theta_0 = 0.1$, $\varphi_0 = 0$; curve 3 – $\theta_0 = 0.1$, $\varphi_0 = 0.1$. Design parameters of the fields are listed in table 1.

conditions; yet, at some time, the system seems to 'recall' its initial state and abruptly changes its trajectory. The functions $\theta(\tau)$ behave similarly.

The frequency spectrum (we have chosen the absolute value of the Fourier-spectrum $|F[\varphi(\tau)]|$) of the solutions close to stochastic ones, becomes broad-band, and an example ($N_x \neq N_y = N_z$) is given in figure 9. It is seen from this figure that in the range of the difference ($\Delta N = N_x - N_y$) and sum ($N_x + N_y$), distinct peaks in the frequencies are observed, the amplitude of the difference harmonics being 8 to 10 times greater than the amplitude of the sum harmonics. At high values of δ, the time dependences $\theta(\tau)$ and $\varphi(\tau)$ become more complicated, displaying a periodic behaviour (figure 10).

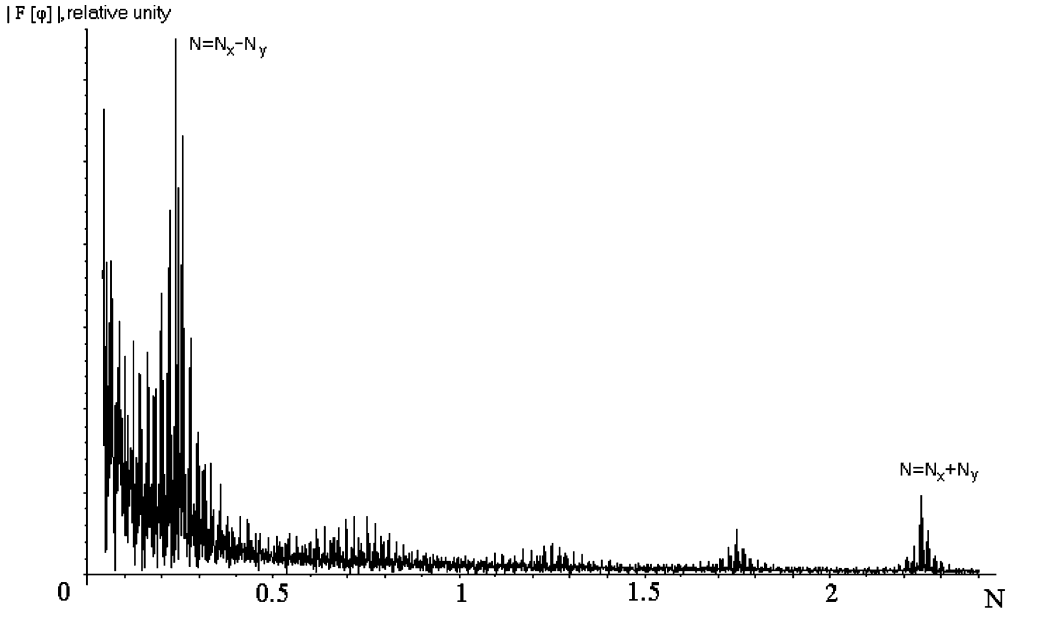

Figure 9. Fourier-spectrum | F [φ] | dependence on dimensionless frequency for the solution shown in figure 7.

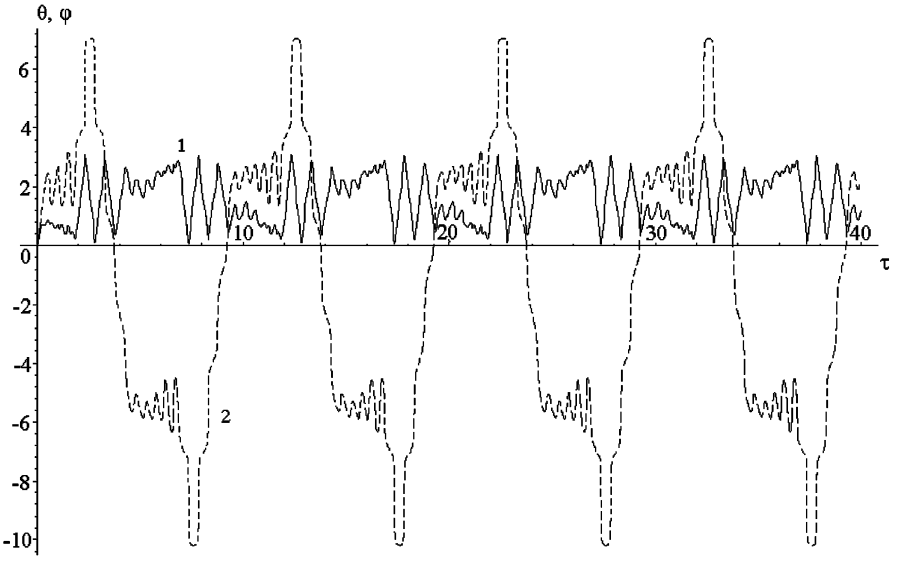

Figure 10. Dependence of the polar angle θ in radian (curve 1) and azimuth angle φ (curve 2, dotted line) of the director orientation on dimensionless time. Design parameters of the fields are listed in table 1.

The Fourier spectrum (see figure 11) becomes less broken, with distinct equidistant harmonics, spaced apart by $2\Delta N$, emerging in it. The transmission functions $T(\tau)$ of the sample in the stochastic regime calculated from equation (24), are more chaotic in general appearance (figure 12, the fragment of the transmission function) than the initial solutions $\theta(\tau)$ and $\varphi(\tau)$. This is caused by the extra non-linear dependences in the transmission function itself (24).

The design trajectories of the motion in the plane in the phase space, and Fourier spectra of the transmission function corresponding to these trajectories, are shown

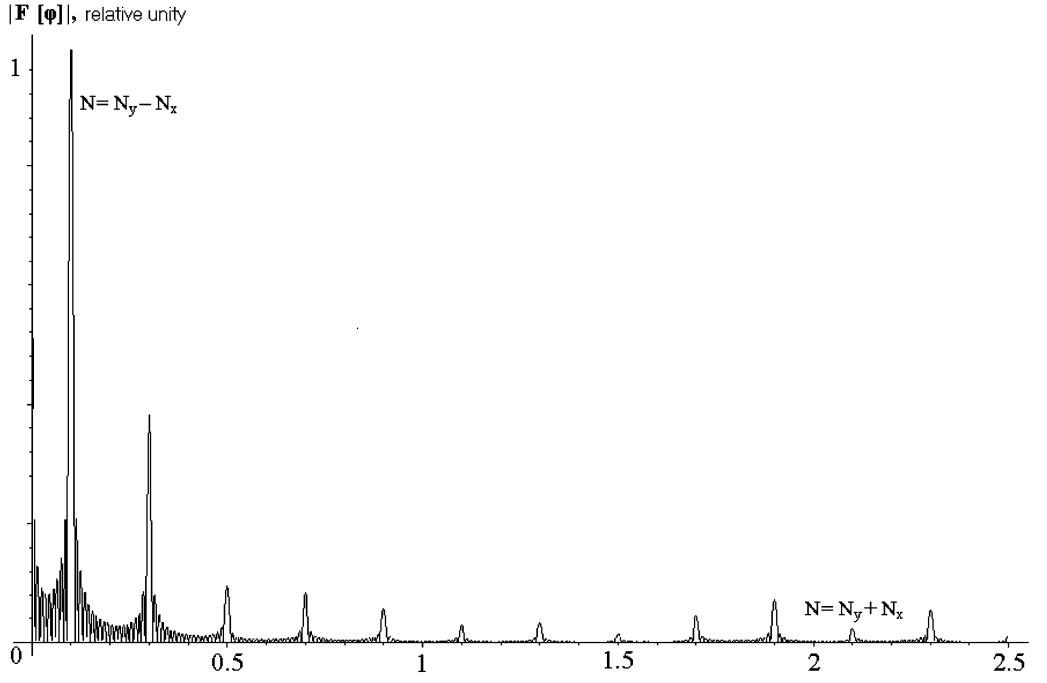

Figure 11. Fourier-spectrum |F [φ]| versus dimensionless frequency for the solution shown in figure 10.

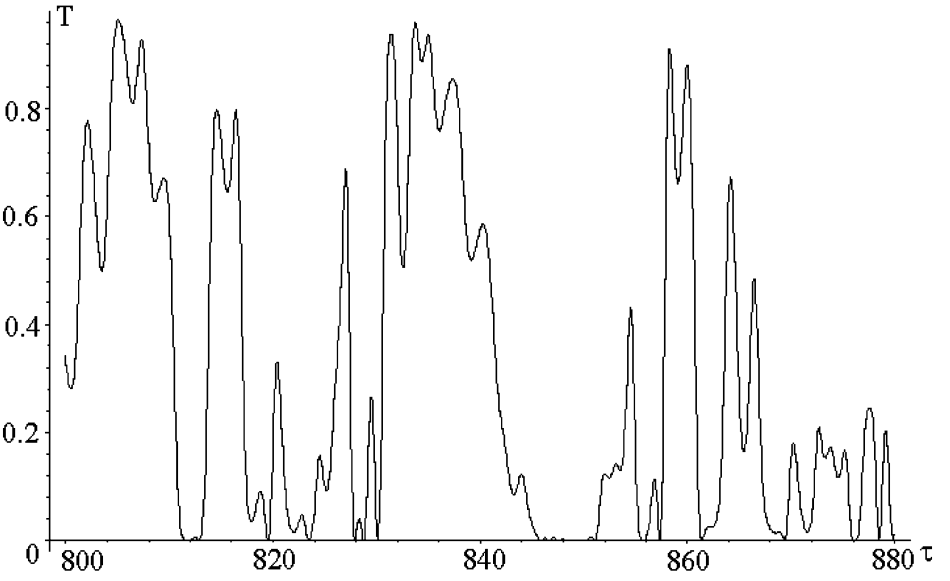

Figure 12. A fragment of the transmission function in relation to dimensionless time. Design parameters of the fields are listed in table 1.

in figure 13. Similarly to the solutions of $\theta(\tau)$ and $\varphi(\tau)$, the phase trajectories present very complex shapes. The spectral functions $|F[T(\tau)]|$ have characteristic lines, figures 13 (*b*, *d*). The appearance of stochastics is indicated by the noise component as the frequences approache zero, figures 13 (*d*, *f*), and in the summary frequencies region. The volumetric reorientation, $\varphi(\tau) \neq 0$, $\theta(\tau) \neq 0$, which appears under the action of a three-component field on the NLC, complicates the spectral characteristics of the transmission function (24), in particular, low frequency lines appear.

Note that the solutions presented here by no means exhaust all dynamic orientational behaviour that can be derived from equation (22). It is impossible to give a complete description of all regimes in one article, because the initial parameters are too large in number (in the case under consideration, with allowance for normalization, a total of seven parameters is to be dealt with).

A preliminary analysis showed that, above all, for non-determinate solutions to be obtained, the bulk deformation of NLC orientation or involvement of all the three field components, $E_x \neq 0$, $E_y \neq 0$, and $E_z \neq 0$, is necessary. This conclusion also follows from the mathematical statement that predicts no stochastic solutions to exist for the systems governed by just one first order ordinary differential equation [16]. With one component being zero among the three field components, in the steady state regime, system (12) reduces to one equation for the deviation angle of the director that lies in the variation plane of **E**. Moreover, it is necessary that the electric fields contain components of at least two different frequencies: $\omega_i \neq \omega_j = \omega_k$, $i, j, k = x, y, z$, $i \neq j \neq k$.

5. Description of the experiment

In the experiment we used as NLC a mixture of 5CB and MBBA. The cell shown in figure 14 (*a*) contained two parallel flat glass plates. The gap L between them depended on calibrated insertions of teflon. The inner surfaces of the plates were coated by the electrode system, which is shown in figure 14 (*b*). The electrode configuration consisted of two crossed electrode groups. The first comprised three parallel stripes of width $D = 1$ mm, with gaps between of $d = 0.2$ mm, set on one plate (designated as 1, 2, 3 in the figure). Asimilar grouping was set on the another plate (4, 5, 6). The standard ITO mixture was used for the transparent electrodes. We realized a simplified technological version with so-called in-plane-switching (IPS) [17]. When assembling, the electrode stripes of the top and bottom glasses were oriented perpendicularly. The external variable voltages were supplied from generators to realize electric fields as follows: on electrodes 1 and 2, along the x-axis, on electrode 4 and 6, along they y-axis, and on electrodes 2 and 5, along the z-axis. The electric fields in the inter-electrode space are defined as $E_x \sim U_x/D$, $E_y \sim U_y/D$, $E_z \sim U_x/L$. To obtain comparable fields inside the sample, E_x, $E_y \sim E_z$ at a given value of D; a gap thickness $L = 150\,\mu$m proved to be optimum. Experiments were also carried out with other values of

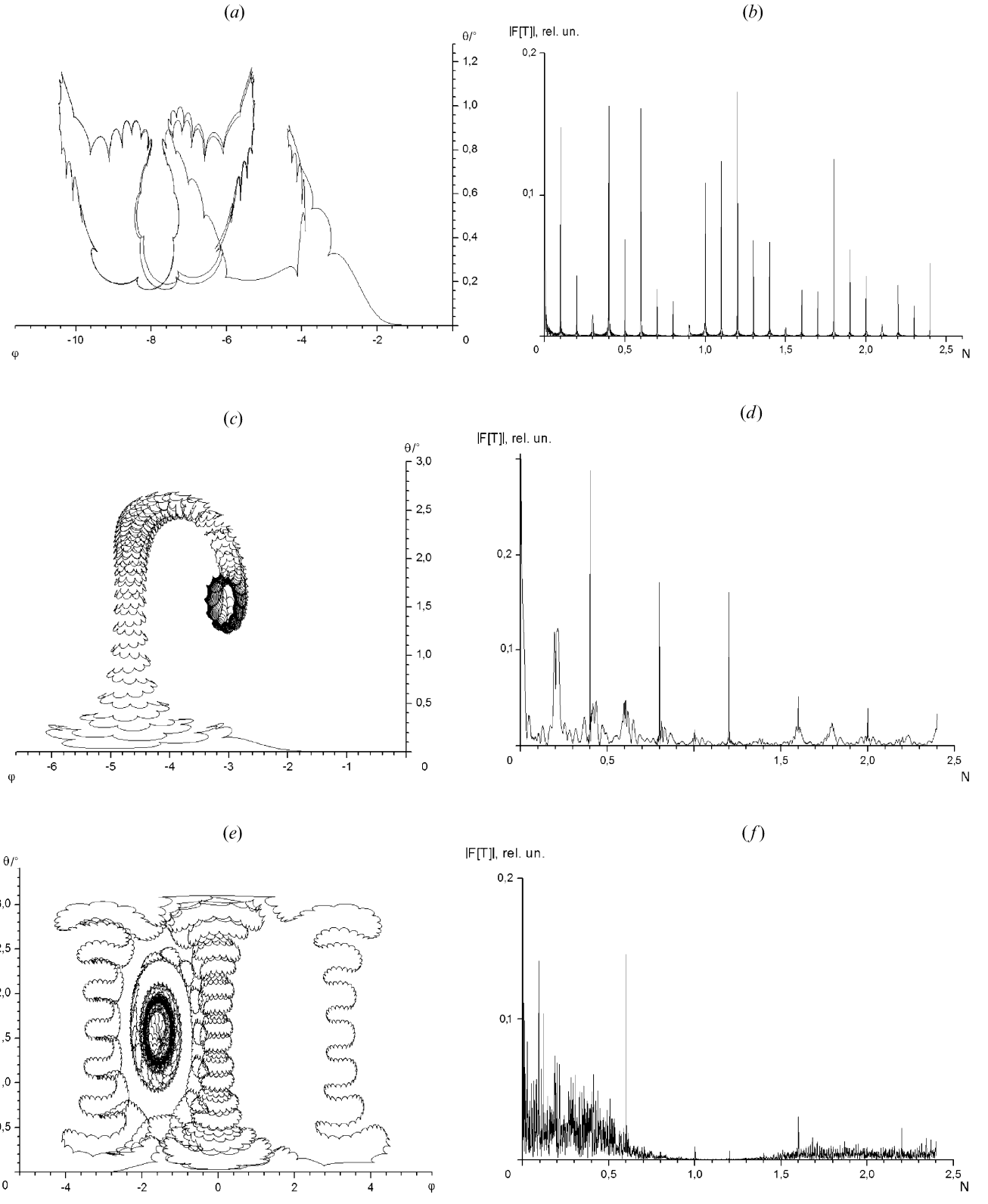

Figure 13. (*a*, *c*, *e*) Trajectories of motion in the plane $[\theta(\tau), \varphi(\tau)]$ in radian; (*b*, *d*, *f*) corresponding spectral transmission functions. Design parameters of the fields are listed in table 1.

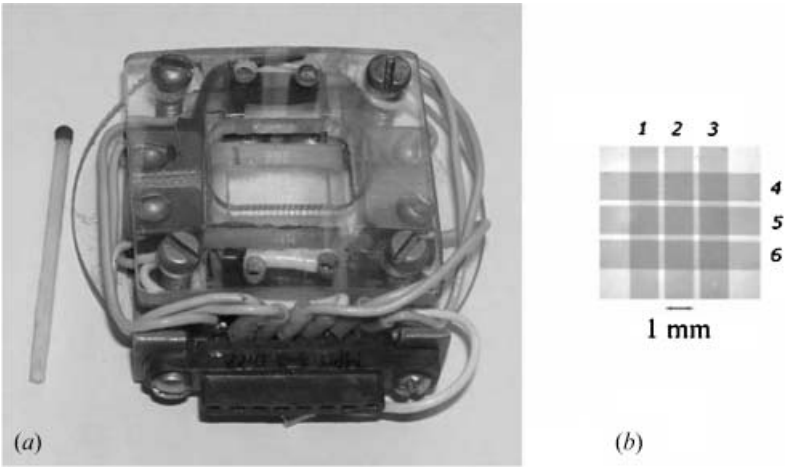

Figure 14. (*a*) The appearance of the NLC sample used in the experiments. (*b*) Enlarged photograph of the electrode system: numbers 1, 2, 3 denote electrode stripes on the bottom glass plate; 4, 5, 6 denote stripes on the top plate.

L in the range 10–150 μm. The experimental data given below were obtained mainly on 150 μm samples. The applied voltages did not exceed the mean-square values for U_x, $U_y \sim 150$ V and $U_z \sim 50$ V. The frequency range for the experiments was 10 Hz–5 MHz. The initial orientation of the samples was homeotropical and resulted from the chromalan processing on the glass surface.

To diagnose the state of the NLC orientation (the transmission function T vs time t), the sample was illuminated by a focused beam ($f=30$ cm) of a semiconductor low power laser ($\lambda=0.647$ μm, controlled output 1–10 mW). An analyser and photodetector (photomultiplier tube of photodiode) were set in the path of the radiation. To visualize the slow changes of the transmitted and dispersed light, the photodetector was replaced with a dull screen. To obtain a conoscopic pattern, the laser beam was previously extended by a collimator, and then directed onto the NLC situated in the convergent (divergent) part of the beam through a short focus lens ($f=3$ cm).

The data from the photodetector were received by a digital oscillograph (BORDO-221, made as a computer expansion card), combined with a spectrum analyser. In the general case, the experiment involved three digital generators (computer expansion box AGENT B-230), These could operate either independently, when U_{x0}, U_{y0}, U_{z0}; v_x, v_y, v_z were assigned; or in a mode with two or three similar frequencies with the given phase shift $\psi_{ij}=\psi_i-\psi_j$ ($i, j=x, y, z$; ψ_x, ψ_y, ψ_z are the phases of the corresponding signals in the range from 0 to $\pm 180^\circ$) between the one-frequency voltages. To obtain a increased voltages (up to 250 V) on the sample electrodes, we used transformers of the corresponding frequency range. In addition, we provided for constant voltage supplies V_{x0}, V_{y0}, V_{z0} on the electrodes. Each master and diagnosing system was controlled from one computer. In the general case, at the sinusoid voltages on the generators, it was assigned:

$$U_x=V_{x0}+U_{x0}\sin(2\pi v_x\tau+\psi_x),$$
$$U_y=V_{y0}+U_{y0}\sin(2\pi v_y\tau+\psi_y),\ U_z=V_{z0}+U_{z0}\sin(2\pi v_z\tau+\psi_z).$$

6. Experimental results and discussion

The photomicrographs in figures 15 (*a–c*) show the conoscopic patterns obtained in the experiment. Figure 15 (*a*) shows the a typical image for an undisturbed homeotropically-oriented sample of the NLC. Figure 15 (*b*) corresponds to a rotating 2D field, $U_{x0}=U_{y0}=98$ V, $U_{z0}=0$ V; $v_x=v_y=3$ kHz, $\psi_{xy}=\psi_x-\psi_y=90^\circ$. Figure 15 (*c*) corresponds to astationary sinusoidal electric field with parameters $U_{x0}=U_{y0}=70$ V, $U_{z0}=0$; $v_x=v_y=3$ kHz. In these cases, unless otherwise specified, the fixed bias of the voltage is equal to zero ($V_{i0}=0$). We obtained a large number of varying conoscopic patterns, their appearance depending on almost every parameter governing the electric fields in the sample. These time-averaged images hardly give quantitative information, and hence in this paper we have restricted discussion to the two the most typical patterns. In the case of Fréedericksz re-orientation from the homeotropic state into the planar state, one observes the smooth transition of the cruciform image into a pattern consisting of hyperbolas [18]. The complex structure of the produced images (Figure 15 *b*, *c*) vindicates the spatial nonuniformity of the director's and electric field orientation in the region of electrodes 2 and 5 crossing, see the NLC sample, Figure 14 (*b*). The time of the conoscopic pattern onset after the voltage initiation is about 0.5–5 s. Upon this,

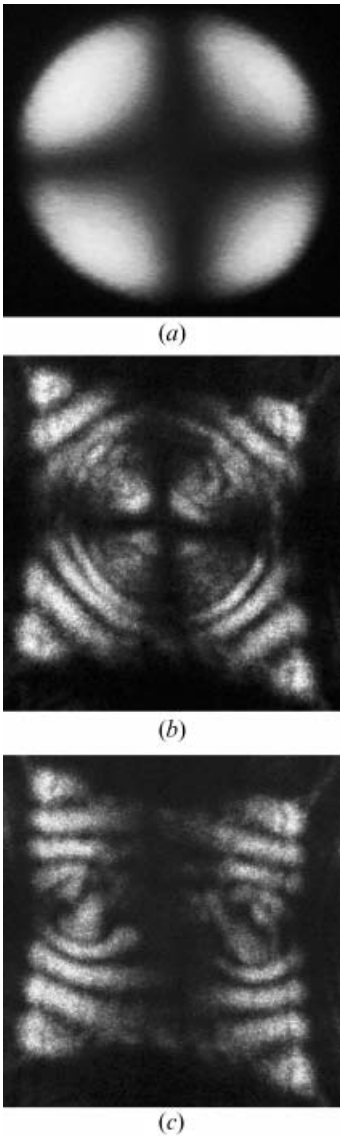

Figure 15. Photomicrographs of the conoscopic patterns for 5CB. (*a*) The image of the undisturbed sample; (*b*) the sample under the action of a 2D rotating field; (*c*) the electric field has constant direction along the image diagonal. The onset parameters of the fields are given in table 2.

the image remains invariable for an arbitrary long period. Such an onset (though the patterns themselves are different) is also observed at the low frequencies, up to 10 Hz. At even lower frequencies, the patterns start to oscillate visibly. At the low frequencies the electrohydrodynamics is more likely to effect the pattern (see also table 2).

To measure the transmission function, the central part of the NLC sample (crossing area of electrodes 2 and 5) was set in the focal waist of the probe radiation. The width of the focal waist was $d \leqslant 0.1$ mm, which is one order less than the transverse inter-electrode space $D=1$ mm. The focusing used for observation allowed a reduction in the effect of any non-uniformity appearing crosswise in the NLC orientation. Nevertheless, the transverse structure of the intensity of the light spot passing through the disturbed NLC was retained, but was more uniform than that obtained with a wide beam. The study and of transverse non-uniformities appearing in this experiment is beyond the scope of the present paper, and calls for the individual consideration.

The major quantified experimental findings are the spectral transmission functions $F(v)=|F[T(t)]|$, which are defined as the absolute value of the Fourier-transformation from $T(t)$. This chosen characteristic is preferred to the time functions, because of the broad frequency band of the registered signals and due to the highly differing frequencies present in the spectrum, especially in the near-stochastic modes. As an example, figure 16 shows an oscillogram of the transmission function $T(t)$ with no constant component. It is given for 5CB under the influence of electric fields with frequencies $v_x=3$ MHz, $v_y=5$ MHz, $v_z=4$ MHz, bias voltages of $V_{x0}=V_{y0}=30$ V, $V_{z0}=0$ and peak voltages of $U_{x0}=140$ V, $U_{y0}=120$ V, $U_{z0}=15$ V.

The transmission spectra obtained in the experiments, similar to the numerical modelling (see § 5), are very varied. Only a small section of the frequency dependences, the most interesting for us, is presented. In this paper we make only brief comments; a more detailed analysis of the interaction between the NLC and variable electric fields calls for a more detailed examination.

In the given experimental data, the signal-to-noise ratio in the measurement system did not exceed ~5%. The experimental parameters illustrated by the graphs, are listed in table 2.

Figures 17 and 18 show the transmission spectra obtained when the NLC 5CB sample is affected by electric fields in the sonic range. The variations lie approximately in one plane (x, y). The field parameters were the following: in figure 17, $U_{x0}=U_{y0}=150$ V, $U_{z0}=0$ V; $\nu_x=\nu_y=5$ kHz, $\psi_x-\psi_y=0^\circ$ which correlates to a constant-direction field; in figure 18 (*a*, *b*) $U_{x0}=U_{y0}=210$ V, $U_{z0}=0$ V; $v_x=v_y=5$ kHz, $\psi_x-\psi_y=90^\circ$, which correlates with the field rotating with frequency 5 kHz. The spectral function in figure 18 (*a*) clearly shows a maximum at the doubled frequency of 10 kHz, whereas in figure 17 it is absent. The frequency component caused by the rotation of **n**, is shown in figure 18 (*b*) in the region $v \leqslant 200$ Hz. The calculated rotation peak based on the solution of equations (22), (23) gives a value of ~25 Hz, which agrees with the experimental findings in the order of magnitude. The imaged spectral functions confirm the conclusions of

Table 2. Experimental parameters.

Figure number	NLC type	$V_{x0}:V_{y0}:V_{z0}$/V	$U_{x0}:U_{y0}:U_{z0}$/V	$v_x:v_y:v_z$/kHz	ψ_x, ψ_y, ψ_z/degree
15(*a*)	5CB	0:0:0	0:0:0	—	—
15(*b*)	5CB	0:0:0	98:98:0	3:3:0	0, 90, 0
15(*c*)	5CB	0:0:0	70:70:0	3:3:0	0, 0, 0
16	5CB	30:30:0	140:120:10	3000:4000:5000	—
17	5CB	0:0:0	150:150:0	5:5:0	0, 0, 0
18(*a*, *b*)	5CB	0:0:0	210:210:0	5:5:0	0, 90, 0
19(*a*)	5CB	20:20:0	160:160:0	3800:3800:0	0, 90, 0
19(*b*)	5CB	5:5:0	70:70:0	3.95:4.95:0	—
19(*c*)	5CB	0:0:10	140:180:0	2:1.7:0	—
19(*d*)	5CB	25:0:0	70:140:0	17:20:0	—
20(*a*)	MBBA	0:0:0	70:70:7	2:1.7:1.7	—
20(*b*)	MBBA	0:0:7	100:120:15	20:17:19	—
20(*c*)	MBBA	0:0:6	70:80:15	3700:2600:2900	—
20(*d*)	5CB	25:25:0	150:150:5	1100:2200:3300	—

the analytical solutions of equations (16) and (18), namely the presence of orientation oscillations in the onset mode, when the NLC is affected by a circular electric field ($\psi_x-\psi_y=90^\circ$), and correspondingly their absence when the field direction is fixed ($\psi_x-\psi_y=0^\circ$). The pronounced peak in the spectrum of figure 18 (*a*) at 5 kHz, and the splitting of the rotation peak, figure 18 (*b*), are not explained by the model of equations (13), (14) and (16), which consider the reorientation in one plane (x, y) and vindicate the presence of the 3D deformation, ($\varphi(t, \mathbf{r})\neq 0$, $\theta(t, \mathbf{r})\neq 0$), caused by the non-uniformity of the fields appearing in the NLC, or by the flexoelectric effect.

In figure 19 (*a*), for the MHz range of one-frequency 2D fields ($v=3.8$ MHz, $\psi_x-\psi_y=90^\circ$), apart from the peak at the doubled frequency of the fields ($v=7.6$ MHz), one can clearly see a wide maximum at the peak of $v\sim 300$ kHz. Such a peak is typical for the MHz region, and further study is needed to interpret it. The more detailed analysis must take account of the temperature dependence of the coefficients involved in the task, since NLC reorientation in the conditions

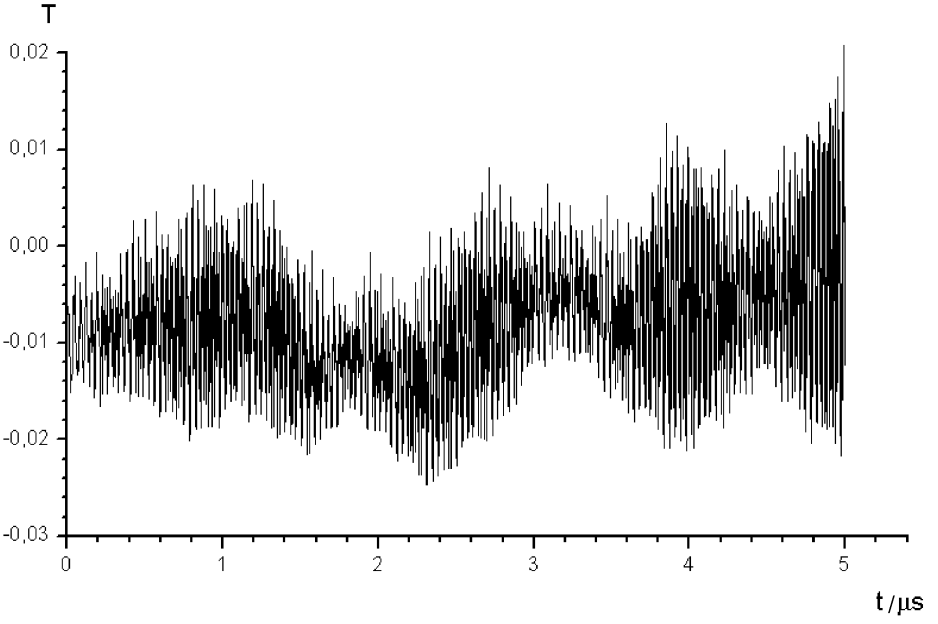

Figure 16. A portion of the experimental dependence of the transmission function (without constant component) on time, when the sample is treated with 3D electric fields in the MHz range. The onset parameters of the fields are given in table 2.

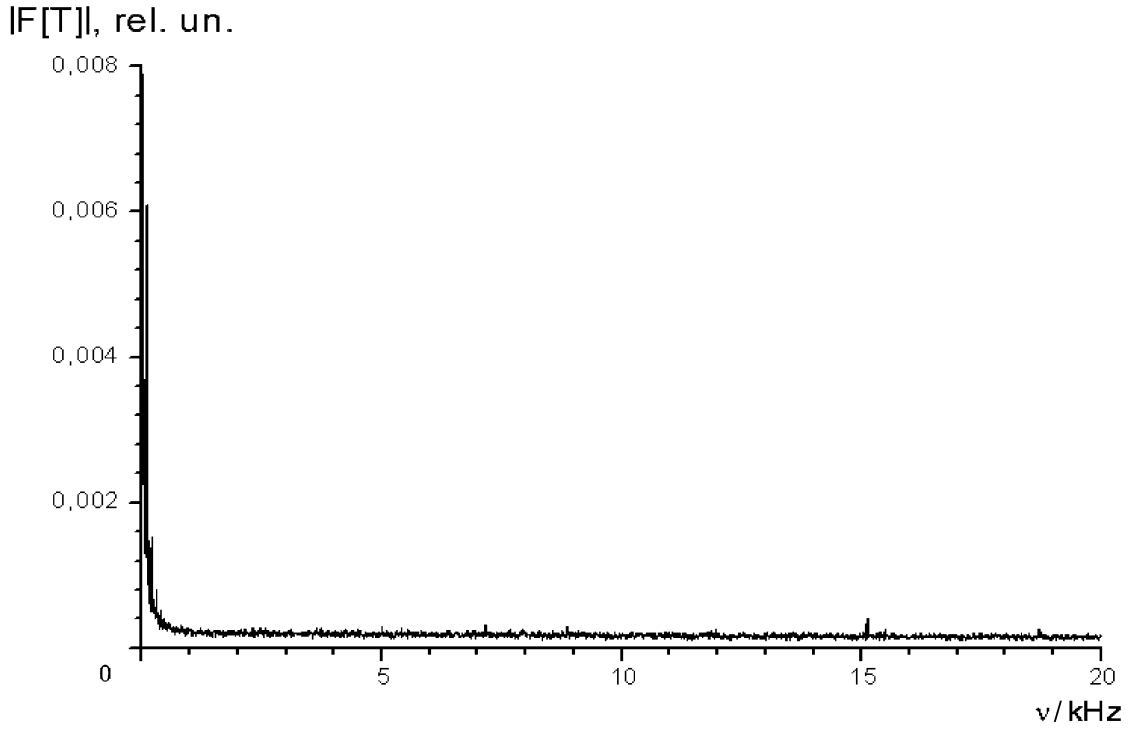

Figure 17. The spectrum of the transmission function of 5CB for a variable field in the sonic range (5 kHz) with constant direction. The onset parameters of the fields are given in table 2.

under consideration progressed with increased release of heat. On observing the sample in a thermal imager, especially in high frequency fields, a temperature rise of 10–20°C was recorded in the interaction zone. This results in a change of viscous coefficients; and rotation frequency, as follows from equation (19), is proportional to the $1/\gamma^2$.

Figure 19 (*b–d*) shows spectra of the transmission functions obtained for different onset values of the 2D fields and frequencies. It should be noted that in the experiments with electric fields it is impossible to obtain a field system without a *z*-component in the sample. This follows from the Maxwell equation (9) for an anisotropic medium, $E_z \sim (\varepsilon_a/\varepsilon_\perp)E_\tau$ and spatial non-uniformity of the electric fields formed in the NLC. The spectral characteristics of the transmission function are more complicated than in the previous one-frequency version. A common property of the spectra presented in figure 19 (*b–d*) is a high peak on the differential (or double differential) frequency, which exceeds the sum frequency peaks, and also the peaks at the frequencies aliquot to the differential frequency. This is in qualitative, and sometimes quantitative, agreement with the results of numerical calculations presented in figures 6, 11 and 13. It is still unclear under what conditions the first maximum peak appears (excluding the zero harmonics) at the frequency $\Delta\nu = |\nu_x - \nu_y|$, figure 19 (*c*), or 2 $\Delta\nu$, figure 19 (*b*). As a rule, the peak at the point $\Delta\nu$ appears if the polarizer and analyser are crossed at an angle χ, see equation (24), which is not aliquot to 45°. In the experiments, $\chi = 90°$; this may be related to the dependence of the vector **n** reorientation dynamics on its initial conditions $\mathbf{n}(t=0)$ (see figure 8).

The interaction between the NLC and three-component and different-frequency 3D fields is more complex. The interpretation of the experimental spectra calls for a more detailed examination, especially in the MHz range of frequencies. Figure 20 (*a*, *b*) shows the transmission function spectrum for acoustic frequencies; the field parameters and type of NLC used are listed in table 2. Figure 20 (*c*, *d*) (parameters in table 2) presents the transmission function spectra for electric fields in the MHz range. We should note the wide noise component in the graphs of figures 19 (*a*), 20 (*c*) and 20 (*d*) within the frequency range 0–2 MHz. It causes transmission function stochastization. In the numerical calculations, a noise component of limited range also appears too, see figures 13 (*d*, *f*). The study of the experimental data for the MHz range is also complicated by the need to take account of the capacity characteristics of the electrode system.

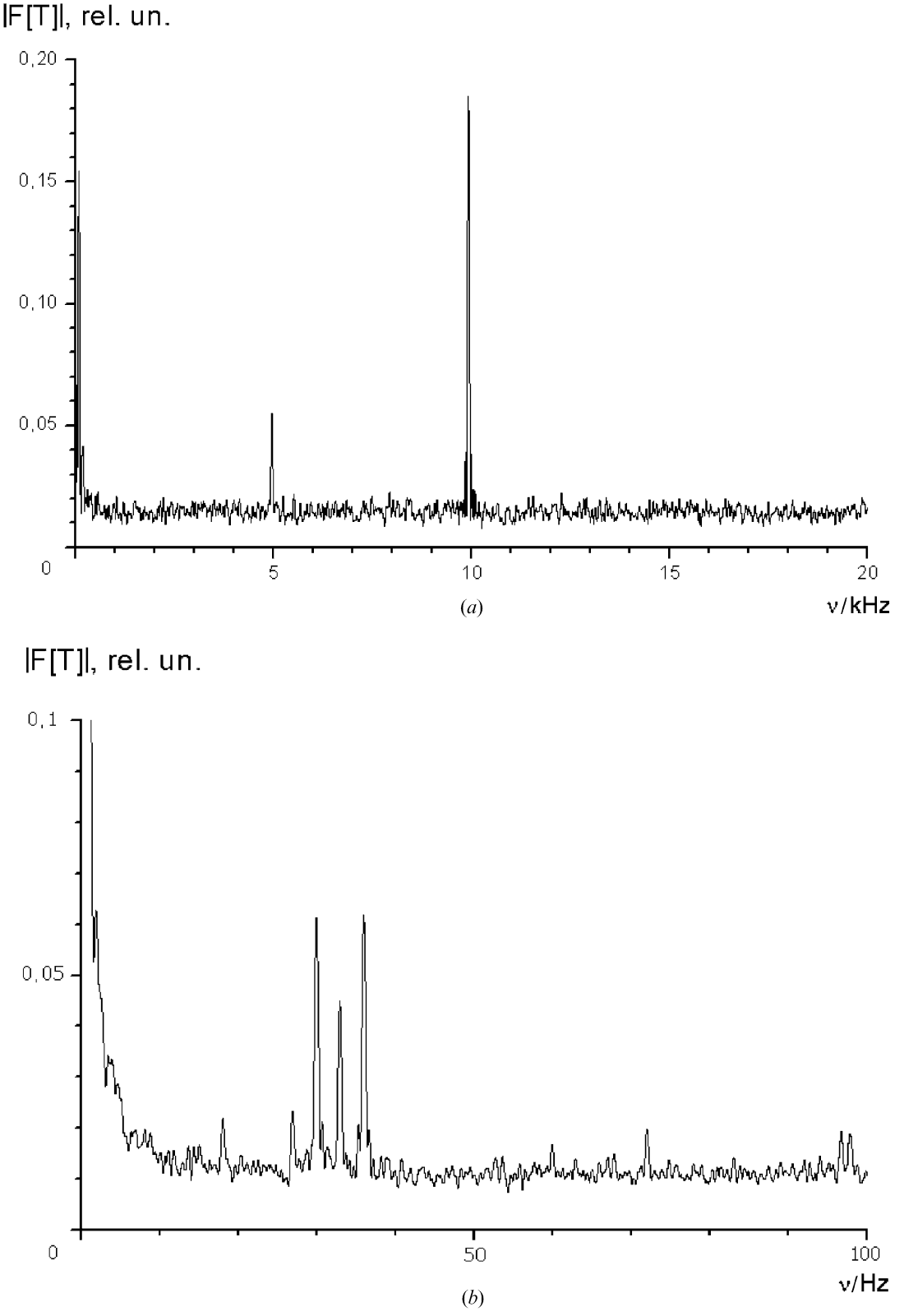

Figure 18. The spectrum of the transmission function of 5CB for a variable field in the sonic range (5 kHz) with 2D rotating direction: (*a*) frequency range $0 \leqslant \nu \leqslant 20$ kHz; (*b*) $0 \leqslant \nu \leqslant 100$ Hz, the frequency region with the peaks responsible for the director rotation. The onset parameters of the fields are given in table 2.

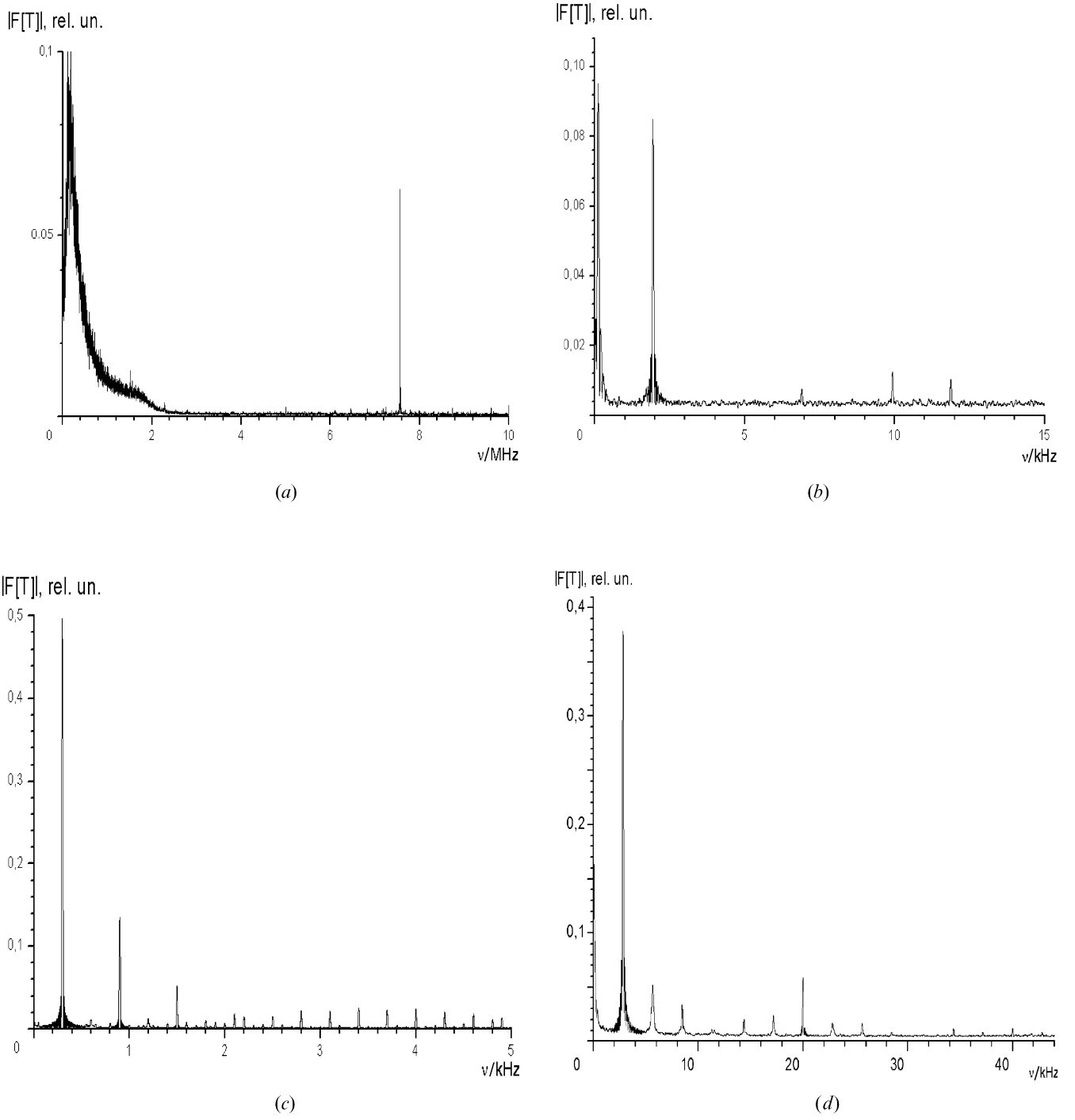

Figure 19. Spectra of the transmission function of 5CB lying in 2D electric fields assigned in the plane (x, y): (*a*) one-frequency 2D rotating field; (*b*, *c*, *d*) two-frequency fields with different directions. The onset parameters of the fields and NLC type are given in table 2.

Many of the spectra under consideration have a common feature, namely the pronounced structure, which consists of individual lines. This agrees well with the calculation results, see figures 11 and 13 (*b*, *d*). The presence of narrow low frequency peaks of $v<\Delta v$, Figure 20 (*b*), depends on the discreteness of the NLC

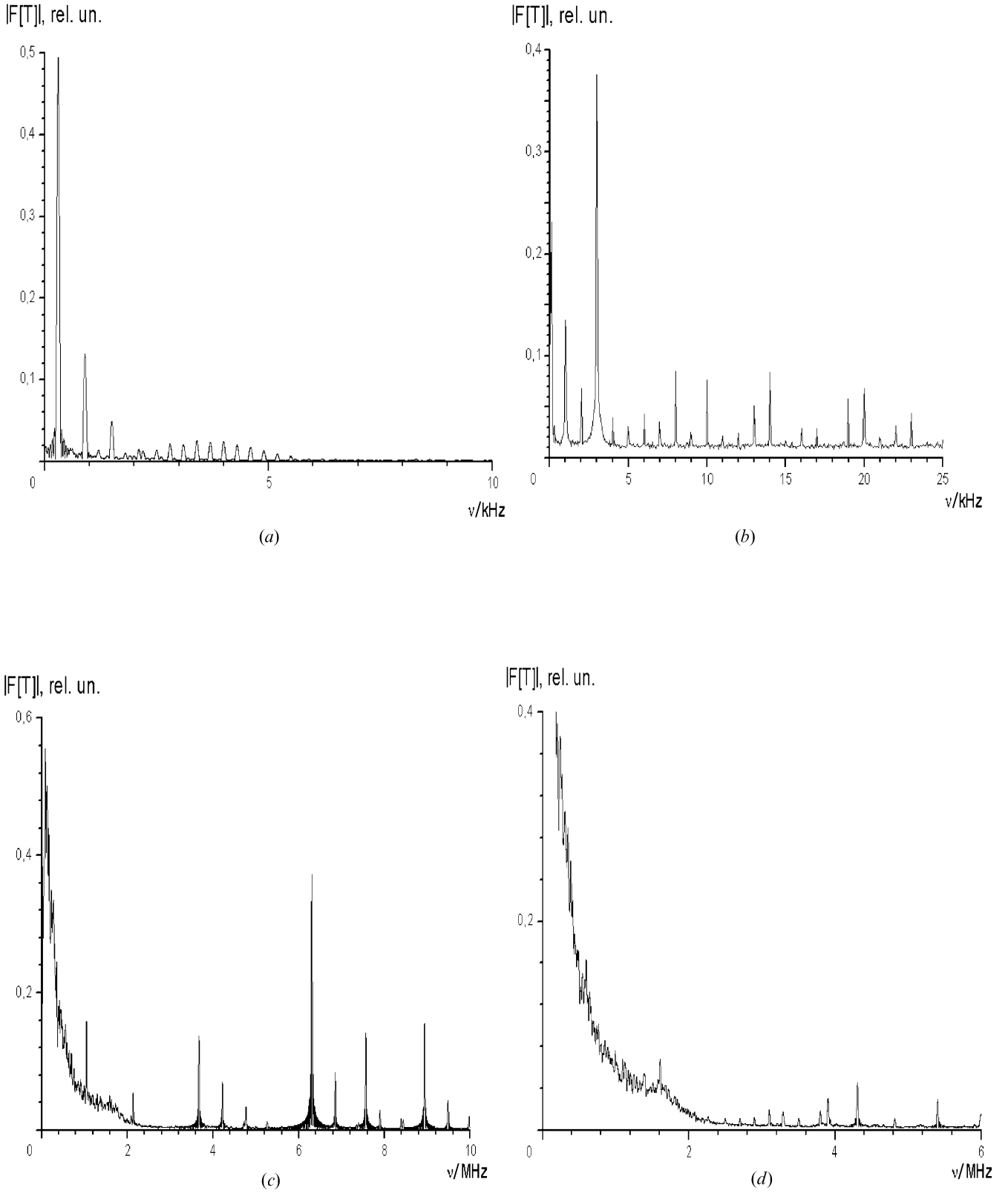

Figure 20. The spectra of the transmission function of a NLC in a 3D different-frequency electric field: (*a*, *b*, *c*) MBBA; (*d*) 5CB. The onset parameters of the fields and NLC type are given in table 2.

director states and on the transitions between these states, which were obtained in the numerical calculations, see figures 7 and 8.

7. Conclusion

The reported experiments with various interactions between multi-component and multi-frequency electric fields and a NLC have yielded qualitative agreement between calculation and experimental findings. The positions of maxima in the frequency characteristics of the transmission functions for 2D geometry of the electric fields are in good quantitative agreement with the theoretically calculated frequency peaks. Theoretically predicted stochastization of the NLC director state has been confirmed experimentally. Oscillation modes of the director orientation at MHz frequencies have been realized.

We failed to obtain strict correspondence between calculated and experimental findings for the approximated model under study. The main reasons for the discrepancy are the neglected elastic forces, spatial dependence of the electric fields, possible appearance of hydrodynamic streams (due to the appearance of low frequency components in the orientation dynamics) and flexoelectric elements. The numerical integration of the equation system in the partial derivatives (6), (9) gave the basis for regard of the spatial dependence of the orientation of **n** (at the first stage, only the effect of elastic forces in the NLC was considered). This resulted in even more complicated and multiple solutions. Further theoretical research into the considered interaction, as well as experimental results will be published later.

From the mathematical viewpoint, the equations studied are the subject of non-linear dynamics theory [16]. The discrete version of the special case of equations (22), (23), after a change of the variables, converts into the situation studied by Grebogy and co-authors in [19]. The equations resulting from this situation approximately describe a system of three non-linear interrelated oscillators. Constructed Poincare cross-sections present an abstract torus map in 4D phase space (θ, φ, θ, φ) on the 2D plane. In [19] the presence of solutions in the form of an irregular attractor is proven on the ground of numerical calculations, and the constructed motion trajectories are similar in complex structure to the corresponding cross-sections obtained in the present paper.

The special property of the attractor behaviour of the solutions, and also the high sensitivity of the discrete version of the equations to the initial conditions and input parameters (for example, in [19] the amplitude and phase additives to equation (23) were chosen arbitrarily) did not allow us to perform an accurate quantitative comparison of the results of [19] and corresponding results of the present paper.

Finally it should be noted that the motive for this fairly detailed study of the described model is the study of the generation of optical harmonics, which appear when polymer media interact with coherent radiation. The attempt to describe numerically the non-linear modes of radiation–NLC interaction has yielded an unexpected result. When analysing the reasons for numerical solution stochastization (stability and accuracy of the applied design models was checked in advance), it was concluded that this effect results from NLC–medium properties, and these properties are described by the constructive equations. Hence, the simplified mathematical model was chosen (Maxwell's equations have been rewritten in an electrostatic form), and nevertheless this model is close to that where the NLC interacts with electric fields up to the MHz range.

The performed numerical and experimental investigations have revealed a new physical subject of non-linear dynamics. This involves a NLC lying in a multi-component variable electric field, and can be described by a dissipative system of ordinary differential equations. This system is one more example among known determined equations, which cause irregular oscillations [16]. The possibility of oscillating behaviour of the NLC orientation with MHz frequencies has been proven. The stochastization of the NLC orientation state must be taken account of during the consideration of liquid crystal–media interaction in the multi-component and multi-frequency electric fields. Rapidly variable orientation states of a NLC are already a feature of liquid crystal engineering [12].

The authors express their gratitude to G. N. Grachev for experimental assistance and to V. F. Kitaeva and A. S. Zolot'ko for helpful discussions. The authors also thank Mr K. V. Dulov, director of 'Optimax' company for support of the investigations. The work was supported by the Federal Integral Researching Program, Russian Federation contract No. 40. 017.1.1.1306.

References

[1] L.M. Blinov. *Electro- and Magneto-Optics of Liquid Crystals* (in Russian), Nauka, Moscow (1978).
[2] Iam-ChoonKhoo. *Liquid Crystals*. Wiley-Interscience Publication, New York (1995).
[3] V.V. Beljaev. *Viscosity of Nematic Liquid Crystals* (in Russian), Fizmatlit, Moscow (2002).
[4] S.A. Pikin. *Structural Transformations in Liquid Crystals* (in Russian), Nauka, Moscow (1981).

[5] N.V. Tabiryan, A.V. Sukhov, B.Ya. Zel'dovich. *Mol. Cryst. Liq. Cryst.* **136**, 1 (1986).
[6] A.S. Zolot'ko, V.F. Kitaeva, N. Kroo, *et al. Zh. eksp. teor. Fiz.,* **87**, 859 (1984).
[7] N.G. Preobrazhenskii, S.I. Trashkeev. *Opt. Spectroscop.*, **62**, 1404 (1987).
[8] A.S. Zolot'ko, V.F. Kitaeva, N.N. Sobolev, *et al., Liq. Cryst.***15**, 787 (1993); G. Demeter, L. Kramer. *Phys. Rev. Lett.,* **83**, 4744 (1999).
[9] V.N. Tzvetkov, *Zh. eksp. teor. Fiz.*, **9**, 603 (1939); V.N. Tzvetkov. *Izv. AN SSSR*, **5**, 57 (1941).
[10] K.B. Migler, R.B. Meyer.. *Phys. Rev. E*, **48**, 1218 (1993).
[11] Ch. Zheng, R.B. Meyer. *Phys. Rev. E*, **56**, 5553 (1997).
[12] Bh.R. Acharya, C.K. Madsen, K.W. Baldwin, *et al. Opt. Lett.,* **28**, 1096 (2003).
[13] S.I. Trashkeyev, G.N. Grachev, V.M. Klementyev, P.A. Statsenko. *Tech. Dig. IV*, p. 262, International Symposium on Modern Problem of Laser Physics, Novosibirsk (2004).
[14] E. Santamato, B. Daino, M. Romagnoli, M. Settembre, Y.R. Shen, *Phys. Rev. Lett.*, **57**, 2424 (1986); A.S. Zolot'ko, V.F. Kitaeva and V. Yu. Fedorovich. *Preprint FIAN N.*, 326 (1986); A. Vella, B. Piccirillo and E. Santamoto. *Phys. Rev. E*, **63**, 031706 (2002).
[15] M. Borne, E. Wolf. *Principles of Optics*. Pergamon, London (1964).
[16] F.C. Moon. *Chaotic Vibrations*. Wiley, New York (1987).
[17] D. Klement, K. Tarumi. Society for Information Displays International Symposium, Annaheim, California, USA, May 17–22, 1998, Digest of Technical Papers. V. XXIX. 393 (1998).
[18] P.G. de Gennes. *The Physics of Liquid Crystals*. Clarendon Press, Oxford (1974).
[19] C. Grebogy, E. Ott, J.A. Yorke. *Physica*, **15D**, 354 (1985).